This article was downloaded by:
On: *26 January 2011*
Access details: *Access Details: Free Access*
Publisher *Taylor & Francis*
Informa Ltd Registered in England and Wales Registered Number: 1072954 Registered office: Mortimer House, 37-41 Mortimer Street, London W1T 3JH, UK

Liquid Crystals
Publication details, including instructions for authors and subscription information:
http://www.informaworld.com/smpp/title~content=t713926090

Non-symmetric dimeric liquid crystals The preparation and properties of the α-(4-cyanobiphenyl-4'-yloxy)-ω-(4-*n*-alkylanilinebenzylidene-4'-oxy)alkanes

G. S. Attard[a]; R. W. Date[a]; C. T. Imrie[ab]; G. R. Luckhurst[a]; S. J. Roskilly[a]; J. M. Seddon[ac]; L. Taylor[ad]
[a] Department of Chemistry, University of Southampton, Southampton, England [b] Department of Chemistry, University of Aberdeen, Old Aberdeen, Scotland [c] Department of Chemistry, Imperial College, London, England [d] School of Chemistry, University of Bristol, Bristol, England

To cite this Article Attard, G. S. , Date, R. W. , Imrie, C. T. , Luckhurst, G. R. , Roskilly, S. J. , Seddon, J. M. and Taylor, L.(1994) 'Non-symmetric dimeric liquid crystals The preparation and properties of the α-(4-cyanobiphenyl-4'-yloxy)-ω-(4-*n*-alkylanilinebenzylidene-4'-oxy)alkanes', Liquid Crystals, 16: 4, 529 — 581
To link to this Article: DOI: 10.1080/02678299408036531
URL: http://dx.doi.org/10.1080/02678299408036531

PLEASE SCROLL DOWN FOR ARTICLE

Full terms and conditions of use: http://www.informaworld.com/terms-and-conditions-of-access.pdf

This article may be used for research, teaching and private study purposes. Any substantial or systematic reproduction, re-distribution, re-selling, loan or sub-licensing, systematic supply or distribution in any form to anyone is expressly forbidden.

The publisher does not give any warranty express or implied or make any representation that the contents will be complete or accurate or up to date. The accuracy of any instructions, formulae and drug doses should be independently verified with primary sources. The publisher shall not be liable for any loss, actions, claims, proceedings, demand or costs or damages whatsoever or howsoever caused arising directly or indirectly in connection with or arising out of the use of this material.

LIQUID CRYSTALS, 1994, VOL. 16, NO. 4, 529–581

Non-symmetric dimeric liquid crystals

The preparation and properties of the α-(4-cyanobiphenyl-4′-yloxy)-ω-(4-*n*-alkylanilinebenzylidene-4′-oxy)alkanes

by G. S. ATTARD, R. W. DATE, C. T. IMRIE†, G. R. LUCKHURST*, S. J. ROSKILLY, J. M. SEDDON‡ and L. TAYLOR§

Department of Chemistry, University of Southampton, Southampton SO9 5NH, England

(*Received 23 June 1993; accepted 10 September 1993*)

Six series of a family of non-symmetric dimers, the α-(4-cyanobiphenyl-4′-yloxy)-ω-(4-*n*-alkylanilinebenzylidene-4′-oxy)alkanes, have been prepared. In three of the series, the number of methylene groups in the flexible alkyl spacer has been varied from 3 to 12 while the terminal alkyl chain is held constant at either 2, 6 or 10. In the remaining series, the effect of increasing the terminal chain length has been studied by holding the spacer length constant at 3, 4 or 5 methylene units while varying the length of the terminal chain from 0 to 10 carbon atoms. The phase behaviour and transitional properties of these series have been investigated using optical microscopy and differential scanning calorimetry, while the structures of the mesophases have been studied using X-ray diffraction on both powder and aligned samples. This study has revealed novel phase behaviour involving intercalated smectic phases stabilized by the mixed mesogenic group interaction. We have identified the first examples of intercalated smectic C, smectic I, crystal B and crystal J phases and have assigned the layer stacking sequences in the crystal B phases. An extension to the current nomenclature used to describe smectic phases is proposed in order to include these new structural modifications such that, for example, S_{A_e}, refers to the intercalated smectic A phase. The specific interaction between the two unlike groups has a much smaller influence on the nematic–isotropic transition temperatures than it has on the structures of the smectic phases. Quantitative estimates of the nematic–isotropic transition temperatures based on the Marcelja–Luckhurst theory provide further evidence for a specific interaction between the unlike mesogenic groups. Finally, the thermal behaviour of binary mixtures of the analogous symmetric dimers is also found to be governed by the mixed core interaction and intercalated smectic phases are observed in these mixtures.

Downloaded At: 10:48 26 January 2011

1. Introduction

There is now a great wealth of molecular architectures known to support liquid crystal behaviour [1]. Of all these, one attracting particular attention is the dimeric structure in which two mesogenic moieties are linked via a flexible alkyl core [2]. This interest stems, in part, from their ability to act as model compounds for semi-flexible main-chain liquid crystalline polymers, but also from their quite different properties

* Author for correspondence.

† Permanent address: Department of Chemistry, University of Aberdeen, Meston Walk, Old Aberdeen AB9 2UE, Scotland.

‡ Permanent address: Department of Chemistry, Imperial College, London SW7 2AY, England.

§ Present address: School of Chemistry, University of Bristol, Cantock's Close, Bristol BS8 1TS, England.

0267-8292/94 $10·00 © 1994 Taylor & Francis Ltd.

to conventional low molar mass mesogens. The vast majority of dimeric liquid crystals reported in the literature may be termed symmetric in that the mesogenic groups are identical. A second class of dimer has been described, however, in which differing mesogenic units are linked and these have been termed asymmetric [3–8]. We feel now, however, that asymmetric is not an appropriate term here, as in a chemical context it might be taken to imply chirality. We propose, therefore, that this class of materials should be referred to as non-symmetric dimers and an example of these are the α-(4-cyanobiphenyl-4′-yloxy)-ω-(4-*n*-alkylanilinebenzylidene-4′-oxy)alkanes,

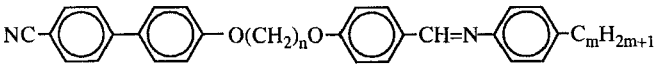

The acronym used to describe this series is CB.O*n*O.*m*, where *n* refers to the number of methylene groups in the flexible spacer and *m* the length of the terminal alkyl chain. The initial report concerning this family of compounds described the CB.O6O.*m* series for which *m* was varied from 0 to 10 [3]. The thermal stability of the smectic A phase exhibited by this series was very unusual in that members with long and short terminal chains exhibited smectic behaviour, whereas for intermediate values of *m* no smectic behaviour was observed. This surprising observation was rationalized by proposing a novel intercalated structure for the smectic A phase exhibited by short chain lengths and a conventional interdigitated structure for long chain lengths. The driving force for the intercalated structure was considered to be the mixed mesogenic unit-mesogenic unit interaction, while for the interdigitated phase, the driving force for association was thought to be the electrostatic interaction between the polar and polarizable cyanobiphenylyl groups and the smectic phase resulted from the molecular inhomogeneity produced by the long terminal alkyl chains. In order to investigate this unusual phase behaviour further, we have prepared three more series belonging to this family of compounds, namely CB.O3O.*m*, CB.O4O.*m* and CB.O5O.*m*. In addition, the transitional properties of dimeric liquid crystals are known to be strongly dependent on the length and parity of the flexible alkyl core and therefore, to study the effect of varying the spacer length on this novel smectic behaviour, we have prepared three further series in which the length of the flexible spacer is varied from 3 to 12 while the terminal chain length is either 2, 6 or 10. The acronyms we use to describe these series are CB.O*n*O.2, CB.O*n*O.6 and CB.O*n*O.10, respectively. This particular family of materials has been chosen, in part, because the parent symmetric dimers, the α,ω-bis(4-*n* alkylanilinebenzylidene-4′-oxy)alkanes [9],

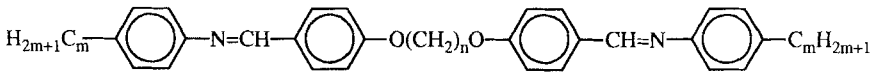

and the α,ω-bis(4-cyanobiphenyl-4′-yloxy)alkanes [2],

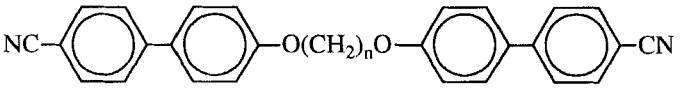

have been studied, thus facilitating comparisons between the non-symmetric and symmetric dimers; the acronyms used for these series are *m*.O*n*O.*m* and BCBO*n*, respectively. We have also studied binary mixtures of the parent symmetric dimers to investigate if the different mesogenic units have to be chemically linked in order to observe intercalated smectic phases.

Downloaded At: 10:48 26 January 2011

2. Experimental

2.1. *Synthesis*

The non-symmetric dimers were prepared via the synthetic route shown in the scheme. The reaction route for the preparation of the three series in which the length of the terminal alkyl chain was varied involved three steps; first, the reaction of 4-cyano-4′-hydroxybiphenyl with an α-chloro-ω-iodoalkane to produce an α-chloro-ω-(4-cyanobiphenyl-4′-yloxy)alkane, **1**; second, the reaction of this with 4-hydroxybenzaldehyde to yield an α-(4-cyanobiphenyl-4′-yloxy)-ω-(4-formylphenyl-4′-oxy)alkane, **3**, and finally, the condensation reaction of this aldehyde with a 4-*n*-alkylaniline to produce the final product, **4**. This route could not be used for the preparation of CB.O*n*O.*m* compounds with $n > 6$ because the required α-chloro-ω-iodoalkanes are unavailable commercially. The synthetic route taken to obtain these materials differed essentially only in the first step in which 4-cyano-4′-hydroxybiphenyl was reacted with a large excess of an α,ω-dibromoalkane to produce an α-bromo-ω-(4-cyanobiphenyl-4′-yloxy)alkane, **2**, which was subsequently reacted with 4-hydroxybenzaldehyde to yield an α-(4-cyanobiphenyl-4′-yloxy)-ω-(4-formylphenyl-4′-oxy)alkane, **3**.

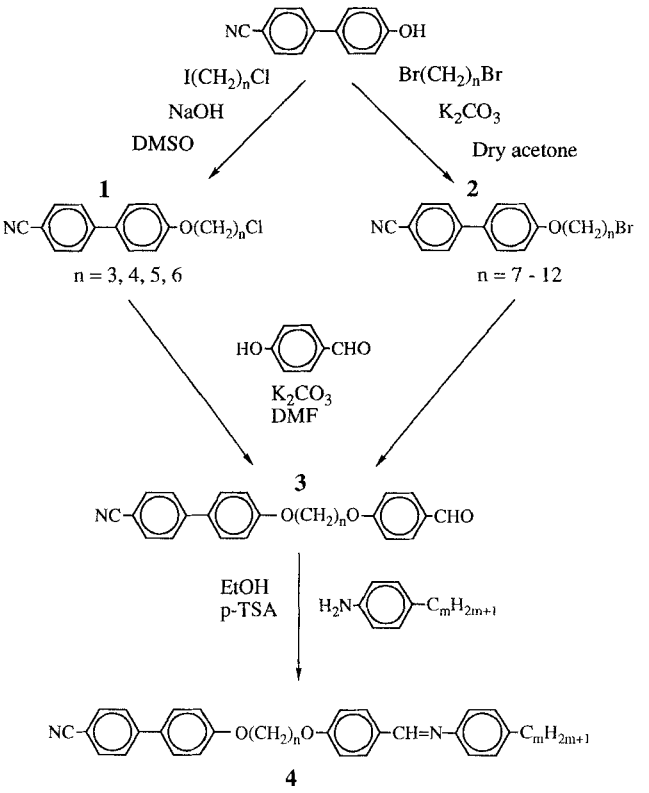

2.1.1. *Synthesis of α-chloro-ω-(4-cyanobiphenyl-4′-yloxy)alkane*, **1**

A mixture of an α-chloro-ω-iodoalkane (0·037 mol), 4-cyano-4′-hydroxybiphenyl (0·035 mol, 6·8 g) and sodium hydroxide (0·035 mol, 1·4 g) in dimethylsulphoxide (40 ml) was stirred at room temperature overnight. The reaction mixture was shaken thoroughly with water (300 ml); the resulting white precipitate was filtered off, washed

Downloaded At: 10:48 26 January 2011

with water and dried. The crude product was passed through silica gel using dichloromethane as eluent and recrystallized from ethanol. The yields of white crystals were in the range 65 per cent to 78 per cent.

1-Chloro-4-(4-cyanobiphenyl-4′-yloxy)butane ^{1}H NMR ($CDCl_3$) δ 2·1 (m, 2 H, $CH_2C\underline{H}_2$), 3·6 (t, 1 H, $C\underline{H}_2Cl$), 4·0 (t, 1 H, $OC\underline{H}_2$), 6·9–7·7 (m, 4 H, aromatic H). IR ν 2210 (C≡N) cm^{-1}.

2.1.2. *Synthesis of α-bromo-ω-(4-cyanobiphenyl-4′-yloxy)alkane*, **2**

The reaction of 4-cyano-4′-hydroxybiphenyl with a ten-fold excess of an α,ω-dibromoalkane using potassium carbonate as base in dry acetone according to the general procedure of Crivello *et al.* [10], has been described in detail by Imrie *et al.* [8] elsewhere.

2.1.3. *Synthesis of α-(4-cyanobiphenyl-4′-yloxy)-ω-(4-formylphenyl-4′-oxy)alkanes*, **3**

The reaction of an α-bromo-ω-(4-cyanobiphenyl-4′-yloxy)alkane with 4-hydroxybenzaldehyde using potassium carbonate as base in dimethylformamide has been described elsewhere [8]. A slightly modified method was used to react an α-chloro-ω-(4-cyanobiphenyl-4′-yloxy)alkane with 4-hydroxybenzaldehyde. Thus, a mixture of an α-chloro-ω-(4-cyanobiphenyl-4′-yloxy)alkane (0·023 mol), 4-hydroxybenzaldehyde (0·025 mol, 3·1 g), potassium carbonate (0·069 mol, 9·5 g) and a catalytic quantity of sodium iodide (0·0023 mol, 0·3 g) in dimethylformamide was heated under reflux with stirring for 3 h. The reaction mixture was allowed to cool and then poured into water (300 ml). The resulting white precipitate was filtered off, washed thoroughly with water and dried. The crude products were recrystallized twice from ethanol and the yields of white crystals were in the range 65 per cent to 80 per cent. The spectroscopic characteristics of these materials have been given elsewhere [8].

2.1.4. *Synthesis of CB.OnO.*m

The 4-*n*-alkylanilines used in the preparation of the final products were either commercially available and these were redistilled immediately prior to use, or were prepared using standard procedures [11]. A 4-*n*-alkylaniline (2·75 mmol) was added to a stirred solution of an α-(4-cyanobiphenyl-4′-yloxy)-ω-(4-formylphenyl-4′-oxy)alkane (2·5 mmol) and a few crystals of 4-toluenesulphonic acid in hot absolute ethanol. The reaction mixture was allowed to cool slowly and stirred at room temperature for 3 h. The resulting white precipitate was filtered off, washed with cold absolute ethanol and dried. The crude products were recrystallized at least twice from either absolute ethanol or ethyl acetate. The exception to this was CB.O4O.1 for which the recrystallization solvent was toluene. The yields of all these reactions were in the range 70 per cent to 80 per cent.

CB.O5O.4 ^{1}H NMR ($CDCl_3$) δ 0·9 (t, 3 H, CH_3); 1·4–2·1 (m, 10 H, $CH_2C\underline{H}_2$); 2·6 (t, 2 H, aromatic-$C\underline{H}_2$); 4·0 (t, 4 H, $OC\underline{H}_2$); 6·7–7·9 (m, 16 H, aromatic H); 8·3 (s, 1 H, $C\underline{H}$=N). IR ν 1620 (CH=N); 2210 (C≡N) cm^{-1}.

2.2. *Characterization*

The purity of the products at each stage was verified using thin layer chromatography and their structures confirmed by ^{1}H NMR and IR spectroscopy. The thermal behaviour of the CB.O*n*O.*m*'s was investigated using a Perkin–Elmer DSC-2C differential scanning calorimeter interfaced to an Opus PCII computer. The optical textures of the liquid crystal phases were examined using an Olympus BH2 polarizing

Downloaded At: 10:48 26 January 2011

microscope equipped with a Linkam THM-600 heating stage. The phase structures were determined using X-ray diffraction on both powder and aligned samples. For the powder samples a Guinier camera fitted with a bent quartz monochromator (R. Huber, Germany) was used. The monochromator was adjusted to isolate $CuK\alpha_1$ radiation ($\lambda = 1{\cdot}5405$ Å). For oriented samples an Elliot toroid camera was used with nickel filtered $CuK\alpha$ radiation ($\lambda = 1{\cdot}5418$ Å). A GX20 rotating anode generator fitted with a 0·1 mm focusing cup (Marconi Avionics, England) was used. The alignment of the sample was achieved by cooling in the presence of a magnetic field which was produced by a samarium/cobalt permanent magnet with the pole gap set at 2·0 mm resulting in a field strength of approximately 1·5 T. The temperature of the aligned samples was regulated to ± 2°C using a Eurotherm 815 controller, while a purpose built electrical heating block was used for the powder samples. The temperature gradient over the powder samples was estimated to be $<0{\cdot}5$°C and about 1°C for the aligned samples. The intensity profiles of the X-ray diffraction patterns were obtained using a Mark III c microdensitometer (Joyce–Loebl, England).

3. Results and discussion

3.1. *Phase assignments*

Nematic phases were assigned from the schlieren optical texture, containing both types of point singularity, which flashed when subjected to mechanical stress. On cooling the nematic phases of many members of the CB.O*n*O.*m* family, the schlieren texture changed to give regions of focal-conic fan and homeotropic textures. The presence of focal-conic fans implied a layered structure, while the homeotropic alignment indicated an orthogonal arrangement of the director with respect to the layer planes. In consequence, this lower temperature phase is assigned as a smectic A phase. On cooling the isotropic liquid of several homologues, bâtonnets developed which coalesced to form a focal-conic fan texture coexisting with regions of homeotropic texture. Thus, this is assigned as a smectic A–isotropic transition. X-ray studies on both powder and aligned samples confirmed these assignments. Figure 1 (*a*) shows the intensity profile of the X-ray diffraction powder pattern of the smectic A phase of CB.O4O.10; sharp first and second order reflections are evident in the low angle region, while in the wide angle region a broad peak centred at $(4{\cdot}8\ \text{Å})^{-1}$ is present, characteristic of a liquid-like arrangement of the molecules within the layers. The layer spacing for CB.O4O.10 is slightly less than twice the estimated all-*trans* molecular length. On cooling the smectic A phases of several homologues, the focal-conic fan texture became sanded and broken, while a schlieren texture developed in the homeotropic areas. These textural changes are indicative of a smectic A–smectic C transition and this assignment has been confirmed by X-ray diffraction experiments. Figure 1 (*b*) shows the intensity profile of the X-ray diffraction powder pattern of the smectic C phase of CB.O4O.10; sharp first and second order diffraction maxima are present in the low angle region while the wide angle diffraction band is broad. The layer spacing is close to that of the S_A phase. This diffraction pattern alone does not exclude the possibility that this is a smectic A phase, but given the described optical textures, this assignment is unambiguous. The layer spacings, and their temperature dependence, for the smectic A and C phases will be discussed later.

On cooling the smectic A phases of several members of the CB.O*n*O.2 and CB.O*n*O.6 series, the focal-conic fans become lightly crossed by bars which are observed only at the transition and do not persist into the lower phase. The fans in the

Downloaded At: 10:48 26 January 2011

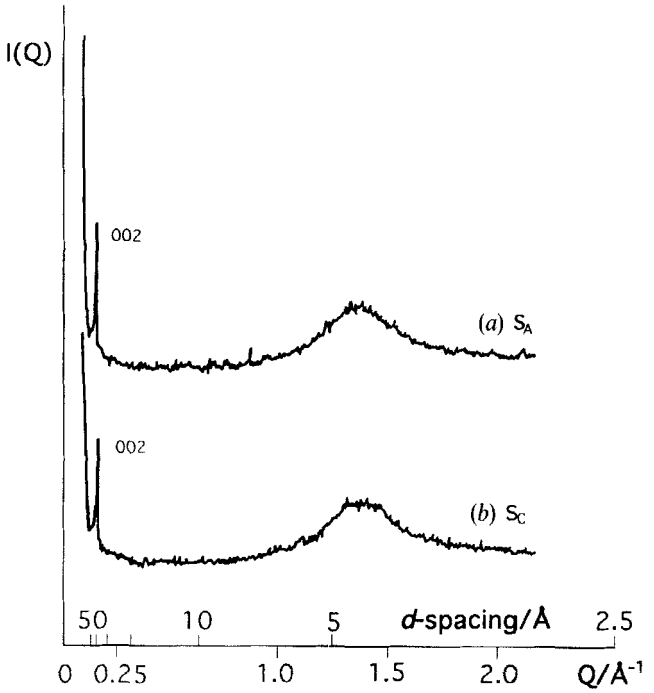

Figure 1. The intensity profile of the X-ray diffraction pattern of (*a*) the smectic A phase at 167°C and (*b*) the smectic C phase at 101°C of CB.O4O.10. The first order (001) layer reflections are over exposed.

Downloaded At: 10:48 26 January 2011

lower temperature phase are smooth and free of blemishes. These textures are shown as figures 2 and 3 and are typical for a smectic A–crystal B transition [12]. X-ray studies have confirmed that the lower temperature phase is a crystal B phase. The textural bands across the fans are thought to arise from the presence of a small biphasic region which is presumably caused by a slight temperature gradient across the sample. It should be noted, however, that we have reported an example in which transition bars accompanied a hexatic B–smectic A transition and thus the observation of transition bars cannot be used to assign a phase as either a crystal or hexatic B as previously thought [9].

On cooling the smectic A phase of the ninth and eleventh members of the CB.O*n*O.2 and CB.O*n*O.6 series and of CB.O11O.10, light lines developed across the fans and schlieren textures of low birefringence developed in the homeotropic regions; these textures are shown as figures 4 and 5. The schlieren texture appears to contain both types of point singularity as can be seen in figure 4. These textural changes are identical to those observed for the seventh, ninth and eleventh members of the NABO*n*O.4 series [4],

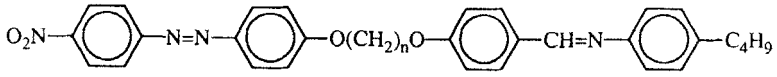

and are very difficult to interpret. The schlieren texture containing both types of point singularity would normally be thought to imply a nematic phase [13]. This assignment is in conflict, however, with the coexisting focal-conic fan regions which indicate that the structure is layered. In addition, the bright threads across the fans suggest a change

in the correlation length normal to the layer planes with respect to the smectic A phase. It has been shown recently, however, that a particular modification of the smectic C phase in which the sense of the tilt angle alternates between adjacent layers exhibits a schlieren optical texture containing both types of point singularity [14]. Figure 6(*a*) shows the intensity profile of the X-ray diffraction pattern of the smectic A phase of CB.O9O.6 and figure 6(*b*) is that of the lower temperature phase. The layer spacings in both phases are close to 0·5 times the estimated all-*trans* molecular length. The fact that only the first order layer reflection is observed indicates that the density profile along the layer normal is close to sinusoidal. It can be seen that on cooling from the smectic A phase, the broad wide angle peak narrows slightly, although it is still much broader than for a hexatic phase, implying some increase in the in-plane ordering of the molecules, while in the small angle region a very small decrease in the layer spacing occurs. However, the decrease in the layer spacing over the whole temperature range of this phase for CB.O9O.6 is only 0·3 Å and this is of comparable magnitude to the experimental error. X-ray diffraction studies on aligned samples revealed that within the resolution of our experiment (tilt angle $\leqslant 8°$) the phase is not tilted; specifically, no splitting of the meridional peaks was observed. Another possibility is that the layers retain their orientation from the preceding smectic A phase and the molecules tilt within the layer although this should be revealed by a significant decrease in the layer spacing at the transition, unless the magnitude of the tilt angle was small. In this arrangement it is difficult to distinguish an aligned smectic C phase from a smectic A phase. The former explanation of a small tilt angle is consistent with both the relatively unblemished fans, see figure 4, as well as with the schlieren texture of low birefringence shown as figure 5, but does not provide an explanation for the unusual schlieren texture. Instead, the structure of the phase is thought to be analogous to that of the antiferroelectric smectic C phase [15] from the standpoint of molecular tilt and will be discussed in some detail later.

Downloaded At: 10:48 26 January 2011

On cooling the smectic C phases of CB.O9O.2 and CB.O11O.2, the schlieren texture changes into a mosaic texture, an example of which is shown as figure 7. X-ray diffraction studies on aligned samples of the phase revealed it to be a crystal B phase. On cooling the crystal B phase of these compounds, the mosaic texture changes to one in which needles cross the mosaic platelets and this is shown as figure 8. These changes in the optical texture suggest that the lower temperature phase is either a crystal G or J phase. X-ray diffraction studies of this phase were not possible because of its monotropic nature and tendency to crystallize.

On cooling the smectic C phase of CB.O9O.6 and CB.O11O.6, a platelet texture developed, see figure 9 and a phase assignment from this alone was not possible. However X-ray diffraction studies on an aligned sample of CB.O9O.6 revealed the phase to be smectic I. Due to the similarity of the optical textures and X-ray powder patterns, the phase exhibited by CB.O11O.6 is considered also to be smectic I. It was not possible, however, to produce a suitably aligned sample of CB.O11O.6 to permit an independent assignment. The X-ray diffraction studies revealed the presence of a crystal J phase below the smectic I phase, although this transition was not detected using microscopy, possibly because of the high viscosity of the compound.

3.2. *The dependence of the transitional properties on the length of the alkyl core*

We turn our attention now to the thermal properties of the CB.O*n*O.*m* compounds and their relationship to the length of the flexible alkyl core. The three series we have

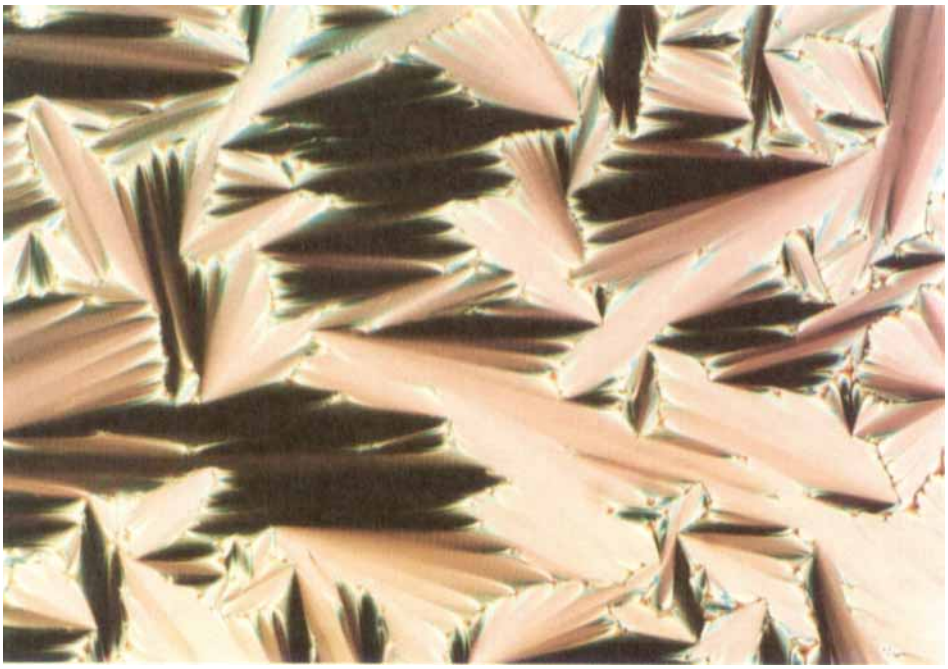

Figure 2. The transition bars at the crystal B_c–smectic A_c transition of CB.O10O.6.

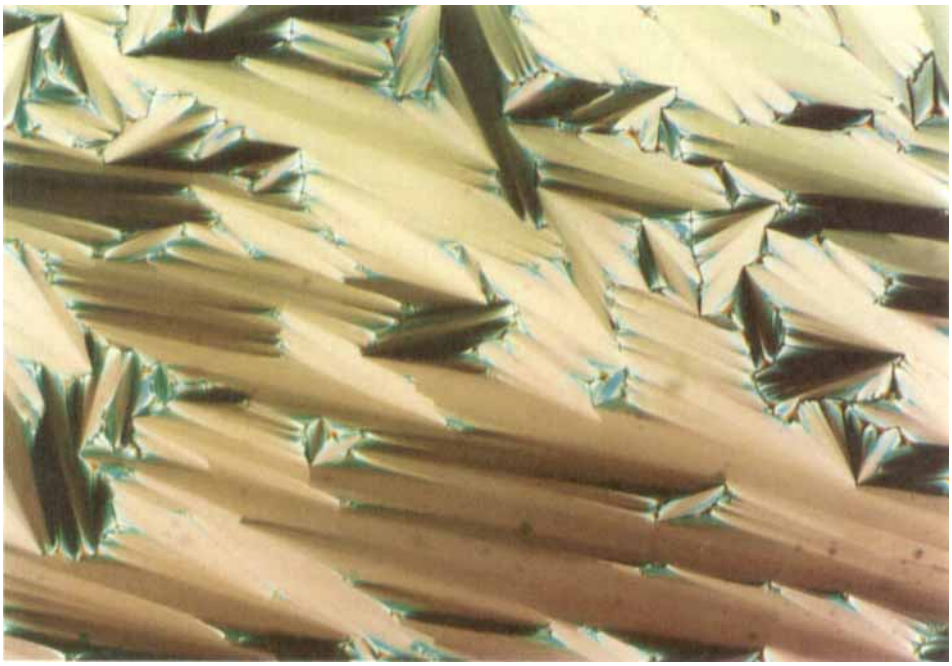

Figure 3. The focal-conic fan texture of the crystal B_c phase of CB.O10O.6 at 100°C.

Downloaded At: 10:48 26 January 2011

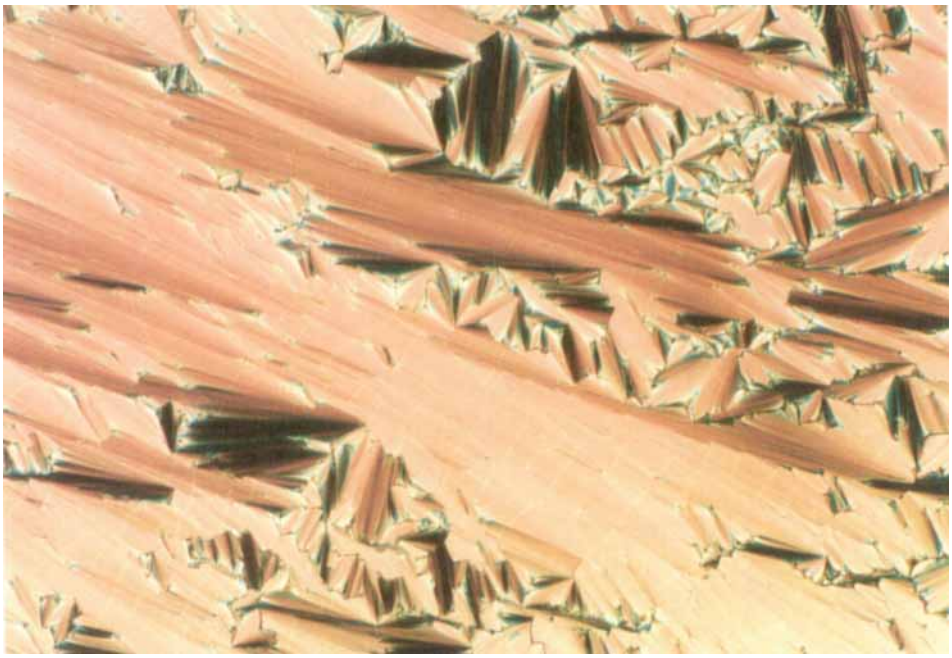

Figure 4. The focal-conic fan texture showing the light lines that develop across the elongated fans on entering the $S_{C_c}^{\dagger}$ of CB.O9O.6 at 108°C.

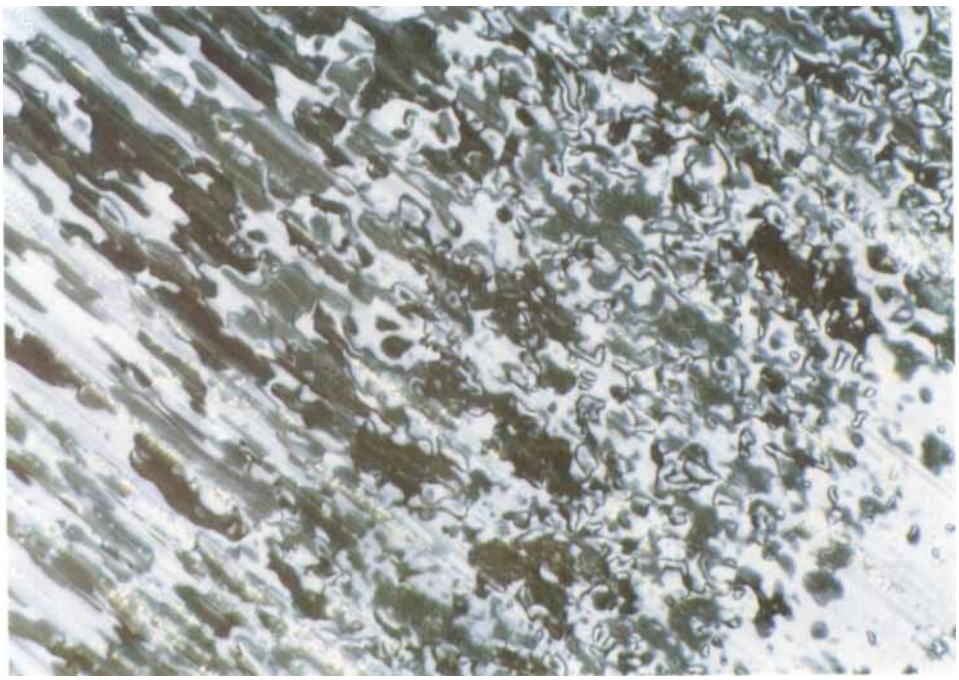

Figure 5. The schlieren texture of the $S_{C_c}^{\dagger}$ phase of CB.O9O.6 at 93°C.

Downloaded At: 10:48 26 January 2011

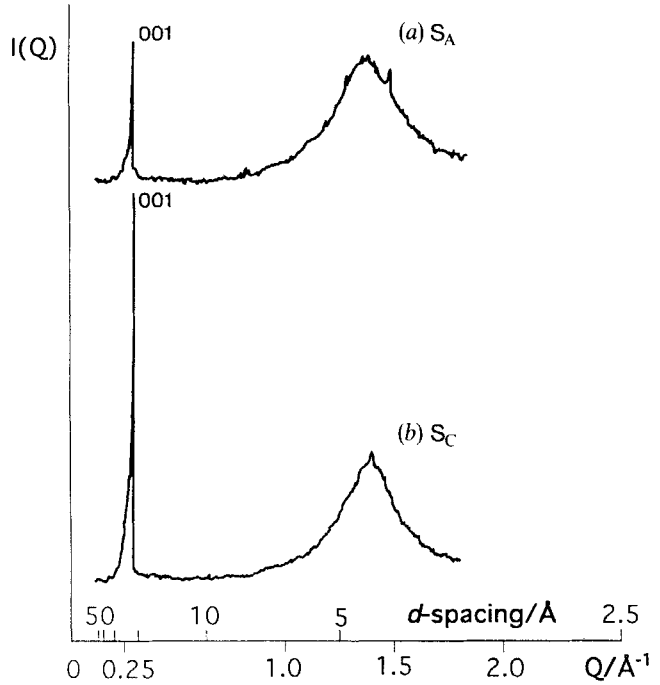

Figure 6. The intensity profile of the X-ray diffraction pattern of (*a*) the smectic A phase at 114°C and (*b*) the smectic C phase at 98°C of CB.O9O.6. The (002) reflections are too weak to be observed.

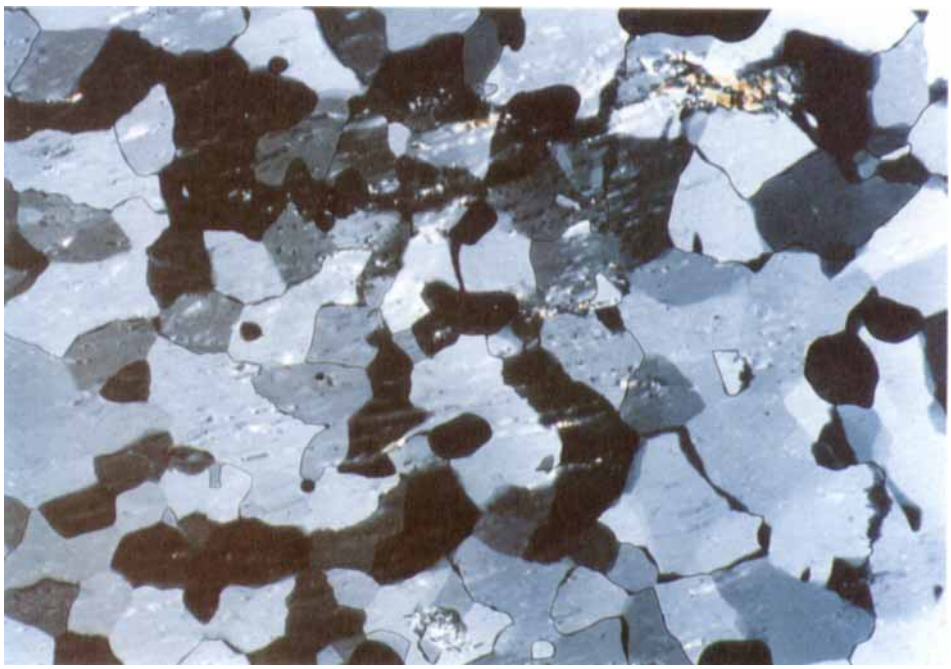

Figure 7. The mosaic texture of the crystal B_c phase of CB.O9O.2 at 101°C.

Downloaded At: 10:48 26 January 2011

Figure 8. The mosaic texture showing needles for the crystal G_c/J_c phase of CB.O9O.2 at 88°C.

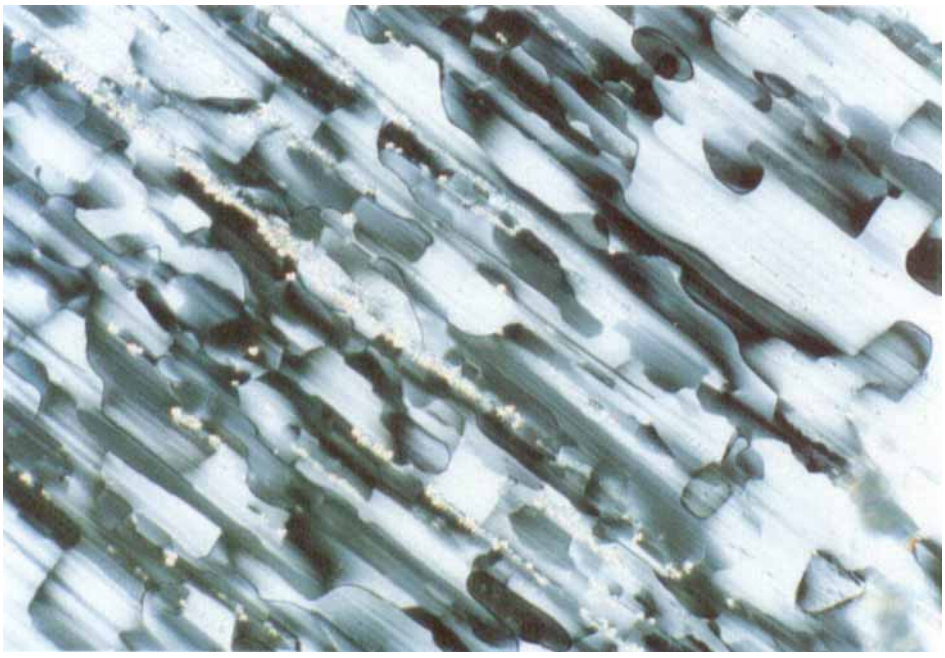

Figure 9. The platelet texture of the smectic I_c phase of CB.O9O.6 at 75°C.

Downloaded At: 10:48 26 January 2011

prepared allow us to consider the effects of the length and parity of the flexible spacer on the properties of compounds having a short terminal chain, CB.O*n*O.2, a medium length chain, CB.O*n*O.6 and finally a long terminal chain, CB.O*n*O.10.

3.2.1. *CB.OnO.2 series*

The transitional properties of the CB.O*n*O.2 series are given in table 1. All ten members of this series exhibit liquid crystalline behaviour, although CB.O3O.2 is a monotropic nematogen. Figure 10 shows the dependence of the transition temperatures on the number of methylene groups in the flexible alkyl spacer. Initially, the

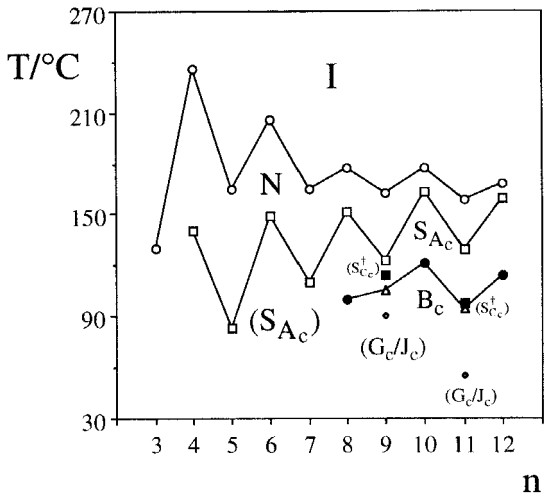

Figure 10. The dependence of the transition temperatures on the number of methylene groups, *n*, in the flexible alkyl spacer for the CB.O*n*O.2 series. The nematic–isotropic transition is denoted by ○, □ indicates the smectic A–nematic transition, ● the crystal B–smectic A transition, ■ the smectic C–smectic A transition, △ the crystal B–smectic C transition and ◇ the crystal G/J–crystal B transition. The melting points have been omitted for the sake of clarity.

Table 1. The transition temperatures of the CB.O*n*O.2 homologous series; ( ) denotes a monotropic transition. All the smectic phases exhibited by compounds having $n \geqslant 8$ have intercalated structures.

n	T_{C-}/°C	$T_{G/JB}$/°C	T_{BS_C}/°C	T_{BS_A}/°C $T_{S_CS_A}$/°C†	T_{S_AN}/°C	T_{NI}/°C
3	145					(130)
4	171				(140)	236
5	107				(83)	165
6	141				149	206
7	143				(110)	165
8	112			(100)	151	177
9	117	(90)	(105)	(114)†	123	162
10	97			121	163	177
11	100	(55)	(94)	(97)†	129	158
12	116			(114)	159	168

Downloaded At: 10:48 26 January 2011

nematic–isotropic transition temperatures exhibit a pronounced alternation as the length of the flexible core is increased with the even members having the higher values, although this attenuates quickly on further increasing n. In contrast, the large odd–even effect exhibited by the smectic A–nematic transition temperatures, T_{S_AN}, is reduced to a considerably smaller extent on increasing n. The general trend in T_{S_AN} for both odd and even members is an increasing one which differs from the general observation for the *m*.O*n*O.*m* family of compounds for which increasing n for any given value of m tends to promote nematic behaviour. In addition, it is interesting to note for the CB.O*n*O.2 series that not only does the thermal stability of the smectic A phase increase on increasing n, but so also does the degree of smectic polymorphism and again this is in contrast to the behaviour of the *m*.O*n*O.*m*'s.

The periodicities measured in the smectic A phase for this series are listed in table 2; unfortunately rapid crystallization prevented X-ray studies on the early members. Table 2 also gives the ratio of the layer spacing, d, to the estimated molecular length, l, obtained from molecular models, and in each case d/l is approximately 0·5. This suggests that the molecules are forming an interleaved structure in which the different mesogenic moieties are overlapping and this has been termed an intercalated smectic A phase. This was found to be formed by other non-symmetric dimers [3, 4] and is sketched in figure 11. This structure has ferroelectric ordering of the molecules, but ferroelectric properties would probably not be exhibited, since it is likely that the molecular groupings would be randomly arranged at the macroscopic level. The intercalated smectic A phase is a new structural modification of the smectic A phase and it is timely, therefore, to extend the existing nomenclature used to describe smectic phases to include these new structural variants. It is logical to refer to them using a subscript c as d is used to refer to the interdigitated modification. Thus, the intercalated smectic A phase, for example, would be referred to as S_{A_c}. As we have noted already, the smectic A_c–nematic transition temperatures exhibit a very large odd–even effect on varying the length and parity of the flexible core and this reflects, in part, the ease with which an even or odd membered dimer may be accommodated into the intercalated structure. The BCBO*n* and 2.O*n*O.2 series do not exhibit smectic behaviour and so it is not possible to make direct comparisons of the behaviour of $T_{S_{A_c}N}$ for the non-symmetric and symmetric dimers. The increasing trend in $T_{S_{A_c}N}$ on increasing n for the CB.O*n*O.2 series is a measure of the ability of the terminal ethyl chain to be located in the space between the intercalated layers which is determined largely by the length of the flexible alkyl core. This is a slightly surprising result, as we might have expected that space would have been filled most effectively in this structure when the terminal chain length was equal to that of the spacer. The observation of intercalated phases for compounds in which the spacer is considerably longer than the

Table 2. The smectic A_c periodicity, d, and the estimated all-*trans* molecular length, l, for the CB.O*n*O.2 series.

n	T/T_{S_AN}	d/Å	l/Å	d/l
8	0·99	18·3	36·6	0·50
9	0·99	18·5	37·4	0·49
10	0·98	19·2	37·9	0·51
11	0·99	19·6	39·2	0·50
12	0·99	20·8	41·3	0·50

Downloaded At: 10:48 26 January 2011

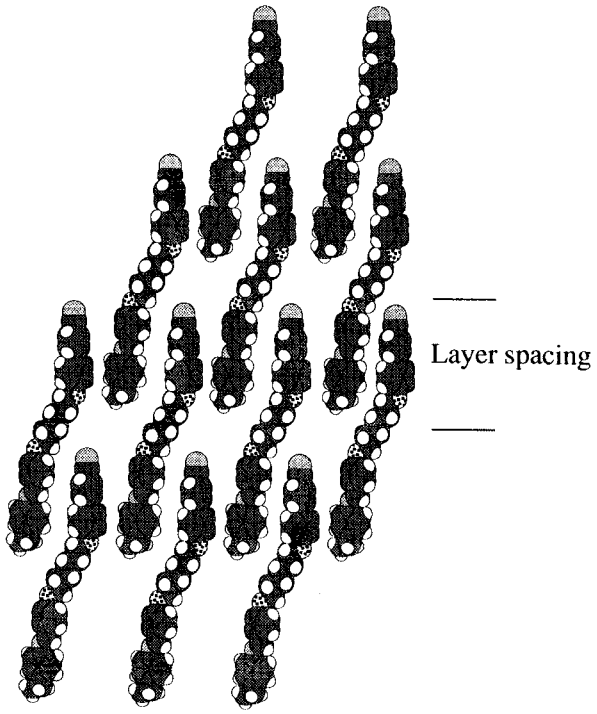

Figure 11. An idealized sketch of the intercalated smectic A phase.

Downloaded At: 10:48 26 January 2011

terminal chain, for example CB.O12O.2, suggests that the translational order in the phase is relatively low and this is confirmed by X-ray diffraction. Smectic phase formation in the CB.O*n*O.2 series may be thought of as a microphase separation into two regions, one consisting of the aromatic cores and the other of the alkyl chains. There exists two possible driving forces for this separation, either the mixed mesogenic unit–mesogenic unit interaction or the poor solubility of mesogenic units in flexible alkanes. An alternative view considers the non-symmetric dimers initially as a mixture of monomers which form the smectic layers. These then have to be linked by spacers and if there is no specific interaction which causes the spacers to fit into the same layer, the intercalated structure is obtained. Indeed, such a randomized arrangement would maximize the configurational entropy of the system. It is interesting to note, however, that for the *m*.O*n*O.*m* series, smectic phase formation involves microphase separation into three regions, such that the aromatic units, flexible spacers and terminal chains each constitute a microphase [9]. It was concluded from this observation that the terminal chain–spacer interaction is an unfavourable one and so prevents the formation of intercalated structures by the *m*.O*n*O.*m* compounds. Indeed, as we have noted already, the 2.O*n*O.2 series are solely nematogens. Thus, for the non-symmetric dimers the smectic phase is presumably stabilized by the mixed core interaction. It is possible also that the mixed mesogenic group interaction actually drives smectic phase formation. The intercalated structure can then be thought to arise from either this interaction offsetting the unfavourable spacer–terminal chain interaction or alternatively, from linking the mesogenic units together in a manner, which does not distinguish between terminal chains and the spacers, in order to fill space most

effectively. Recently, symmetric dimers have been reported which exhibit intercalated smectic phases [14] and these are possibly driven by an interaction between the carbonyl groups which link the spacer to the mesogenic units and the ether groups which connect the terminal chains to the mesogenic moieties.

Simon and his co-workers [16] have described the mesomorphic properties of molecules comprising three chemically different sub-units, for example,

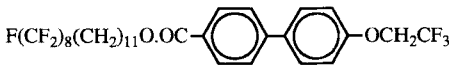

This type of structure can be considered analogous to a non-symmetric dimer in that a rigid perfluoroalkyl chain is separated from a mesogenic group by a flexible spacer. Furthermore, the perfluoroalkyl chain and the spacer are immiscible. The periodicity measured for the smectic A phase exhibited by this compound is approximately equal to the estimated all-*trans* molecular length. This compound also exhibits a more ordered smectic phase and the molecular organization within this phase corresponds to a microphase separation into three distinct regions; mesogenic cores, alkyl chains and perfluoroalkyl chains. Such a separation gives rise to a ferroelectric arrangement of the molecules and in this respect is analogous to the intercalated smectic A phase we have proposed for the non-symmetric dimers. We should note however that Simon and his colleagues [16–18] utilize a segregation of unlike species in order to drive a polar packing arrangement, whereas in our case it is the mixing of the unlike mesogenic units that gives rise to a possibly ferroelectric structure.

In order to investigate the role of the flexible spacer in stabilizing the crystal B phase for which packing constraints should be more pronounced than for the smectic A_c phase, selected examples were studied by X-ray diffraction using aligned samples. The layer spacing measured in the crystal B phase for members of this series corresponds to half the molecular length and to our knowledge this is the first observation of the intercalated crystal B phase. Clearly within the nomenclature we propose this phase would be referred to as the crystal B_c phase. Figure 12 (*a*) shows the X-ray diffraction pattern for an aligned sample of the crystal B_c phase for CB.O10O.2 and figure 12 (*b*) shows the intensity profile along the (001) direction for the layer reflections and for the first (*hk*) ring. The spacings of the Bragg peaks in the wide angle region along the meridional (Q_Z) direction are 1/3 and 2/3 that of the (001) layer reflection in the small angle region. This implies that the layer stacking sequence is of the ABCA type, and in fact the intensity distribution is similar to that previously observed [19]. In contrast, figure 13 (*a*) shows the X-ray diffraction pattern from an aligned sample of the crystal B_c phase exhibited by CB.O11O.2 and figure 13 (*b*) is the intensity profile of this pattern along the (001) direction for the layer reflections and for the first (*hk*) ring. It is clear that the spacings of the Bragg peaks in the wide angle region are 0, 1/2, 1 and 3/2 that of the (001) layer reflection in the small angle region. This indicates that the stacking sequence is of the ABAB type and the intensity distribution is typical for this stacking sequence (see, for example, 4O.8) [19]. Figure 14 (*a*) shows the X-ray diffraction pattern obtained from an aligned sample of the crystal B_c phase of CB.O9O.2 and the intensity profile of this also has Bragg peaks in the wide angle region whose spacings are close to 1/2, 1 and 3/2 that of the (001) layer reflection, but shows no peak on the equator at $l = 0$, see figure 14 (*b*). It is thus probable that the stacking sequence is also of the ABAB type, although the intensity distribution is quite different from that of CB.O11O.2. It would be surprising if the molecular form factor is changed so strongly simply by shortening the

Downloaded At: 10:48 26 January 2011

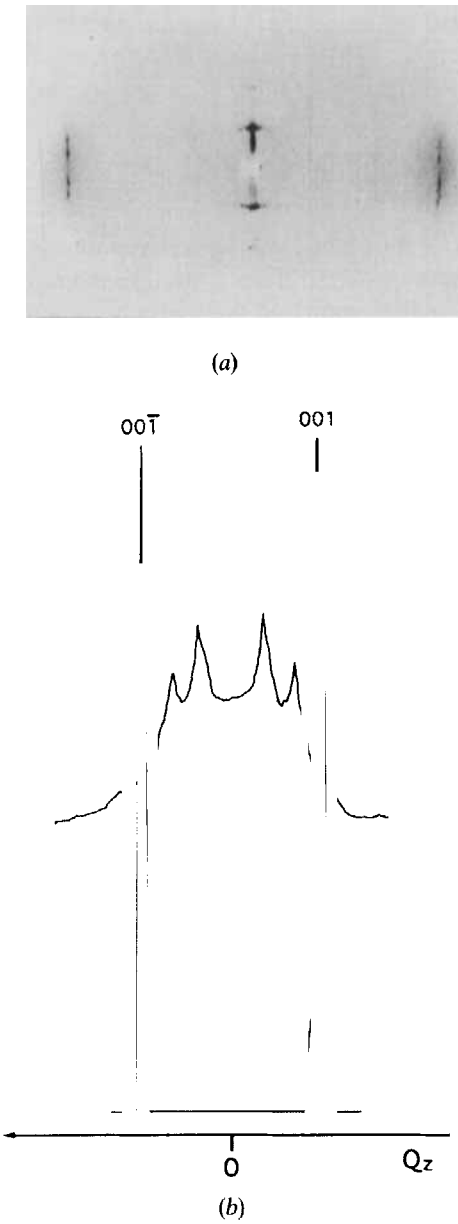

Figure 12. (*a*) The X-ray diffraction pattern of an aligned sample of the intercalated crystal B phase of CB.O10O.2 at 115°C and (*b*) the intensity profile of the pattern along the meridional (Q_z) direction for the (001) layer reflections (lower trace), and for the wide angle ($1, 0, l/3$) peaks (upper trace). The baseline of the lower trace has been offset to omit spurious parasitic scatter around the backstop. Q_z is parallel to the director of the phase.

Downloaded At: 10:48 26 January 2011

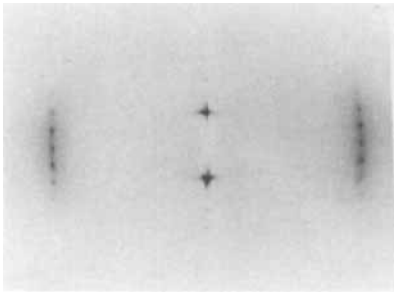

(*a*)

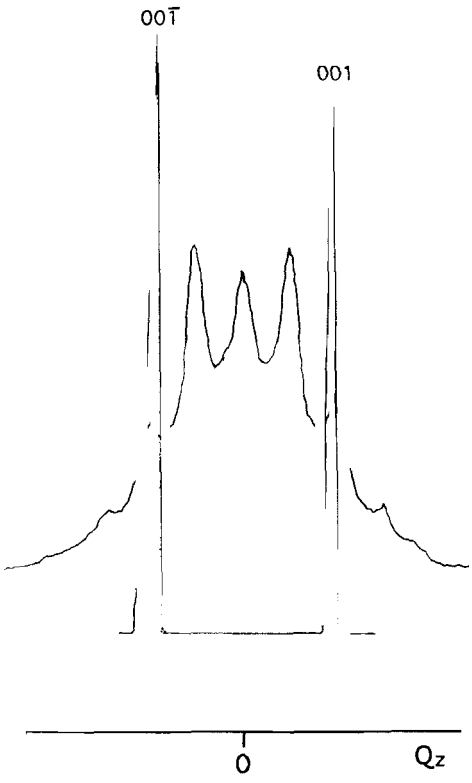

(*b*)

Figure 13. (*a*) The X-ray diffraction pattern of an aligned sample of the intercalated crystal B phase of CB.O11O.2 at 92°C and (*b*) the intensity profile of the pattern along the meridional (Q_z) direction for the (001) layer reflections (lower trace), and for the wide angle $(1, 0, l/2)$ peaks (upper trace). The baseline of the lower trace has been offset to omit spurious parasitic scatter around the backstop. Q_z is parallel to the director of the phase.

Downloaded At: 10:48 26 January 2011

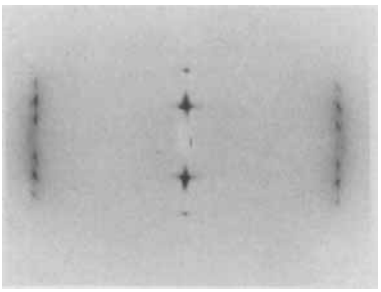

(*a*)

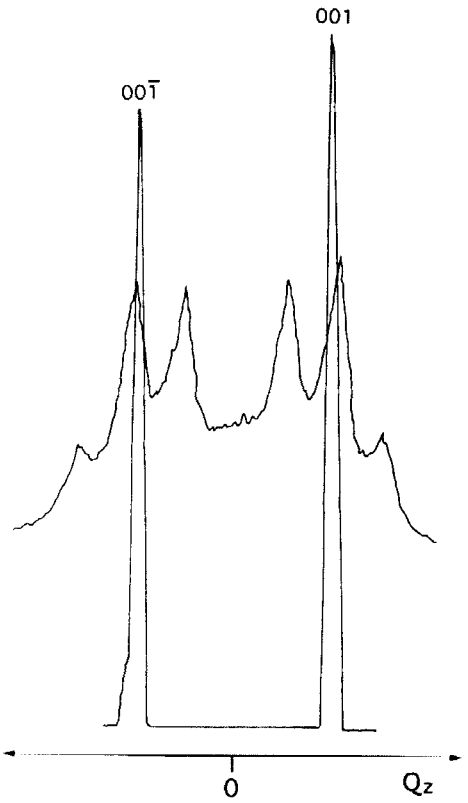

(*b*)

Figure 14. (*a*) The X-ray diffraction pattern of an aligned sample of the intercalated crystal **B** phase of CB.O9O.2 at 104°C and (*b*) the intensity profile of the pattern along the meridional (Q_z) direction for the (001) layer reflections (lower trace), and for the wide angle (1, 0, l/2) peaks (upper trace). The baseline of the lower trace has been offset to omit spurious parasitic scatter around the backstop. Q_z is parallel to the director of the phase.

Downloaded At: 10:48 26 January 2011

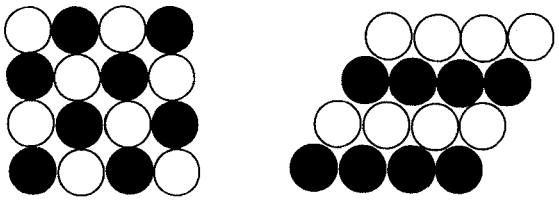

(a) (b)

Figure 15. Two-dimensional packing arrangements based on (*a*) a square planar and (*b*) a hexagonally close packed lattice.

spacer chain by two methylene units, although if the mesogenic groups were tilted in the crystal B phase, the form factor could have a minimum on the equator. Another possibility is that the stacking sequence is not an hexagonally close packed (hcp) structure but one of lower symmetry. For 7O.7, orthorhombic-F and monoclinic-C phases have been observed, where layer B does not occupy the interstitial holes above layer A [20]. The orthorhombic-F phase is difficult to distinguish in low resolution studies from the hcp ABAB structure, although it does give a different intensity distribution along (001) for the wide angle Bragg peaks. Another factor which can cause certain of the wide angle peaks not to be observed for a particular sample orientation is if the sample has long range lattice orientational order. However, this is most unlikely for our sample. It should be noted that there is actually a weak reflection visible in figure 14(*a*) on the equator, slightly further out than the first row of wide angle reflections. This could imply that this phase is a crystal J rather than a crystal B phase. However, in that case the equatorial reflection should be approximately half as intense as the strongest off-equatorial peaks, and additional peaks should also be visible along the Q_Z direction above and below it. Again, these arguments would not hold if the sample had long range lattice orientational order. We have suggested already that the smectic A_c phase exhibited by these compounds is stabilized by the mixed mesogenic unit interaction and it would seem reasonable to assume that this was also the case for the crystal B_c phase. In order to optimize the interactions between the unlike mesogenic groups, it is tempting to suggest that these compounds may form phases possessing a square-planar lattice (see figure 15(*a*)) in which A–B interactions can be maximized, although the packing density is reduced. The X-ray studies, however, show that within a layer the ordering is hexagonal. An alternative packing arrangement, shown as figure 15(*b*), considers alternating rows of A and B particles.

Figure 16 compares the melting points of the CB.O*n*O.2 series with those of the BCBO*n* and 2.O*n*O.2 series and it is immediately apparent that whereas the melting points for the symmetric dimers exhibit a regular dependence on *n*, those of the non-symmetric series do not. We should note that this comparison may be slightly misleading as several members of the non-symmetric series melt to give smectic A phases, while the symmetric dimers undergo crystal–nematic transitions. For any given value of *n*, the melting point of the BCBO*n* homologue (shown as □) tends to be higher than that of the 2.O*n*O.2 member (shown as ●) which in turn is greater than that of the analogous non-symmetric dimer (shown as ○). There are just two exceptions to this, CB.O9O.2 which exhibits a melting point slightly greater than that of 2.O9O.2, while CB.O7O.2 has a melting point higher than either of the analogous symmetric dimers. The general trend, therefore, in the melting points is for the non-symmetric dimers to exhibit melting points which are significantly below the mean of the symmetric dimers (shown as – – –) and this may be considered to be analogous to eutectic behaviour.

Downloaded At: 10:48 26 January 2011

The nematic–isotropic transition temperatures of the CB.O*n*O.2 series are compared to those of the analogous symmetric dimers in figure 17. As we have noted already, the large odd–even effect in the nematic–isotropic transition temperatures for all three series is characteristic behaviour for the majority of dimeric mesogens. Exceptions to this general behaviour include the carbonates [21], for which the geometry of the linking group appears to attenuate significantly the odd–even effect in the transition temperatures. The clearing temperatures of the non-symmetric series are intermediate between those of the symmetric series and with the exception of CB.O8O.2, lie above the arithmetic mean values of the analogous symmetric dimers; these are shown also in figure 17. It is important to stress, however, that these deviations are very small with respect to the transition temperatures themselves. If we make the somewhat simplistic assumption that the mesogenic unit interactions are dominant in determining T_{NI}, then these results suggest that the mixed anisotropic interaction, i.e. the cyanobiphenylyl–Schiff's base interaction, is more favourable, albeit very slightly, than the like interactions, but similar for early members of the series. It is interesting to note that the effective molecular length estimated from the X-ray periodicity measured in the nematic phase which precedes an intercalated smectic A phase is half the all-*trans* molecular length. This suggests that the mixed interaction is responsible also for the deviation from ideal behaviour shown by the nematic–isotropic transition temperatures. By ideal behaviour we mean that the transition temperature of the non-symmetric dimer is equal to the mean transition temperature of the two symmetric dimers. We shall return to a detailed discussion of the observed non-ideal behaviour of this and other series later.

The dependence of the entropies associated with the nematic–isotropic transition on *n* for the CB.O*n*O.2 series is shown in figure 18 and these exhibit a very dramatic odd–even effect. This is archetypal behaviour for a homologous series of dimeric liquid

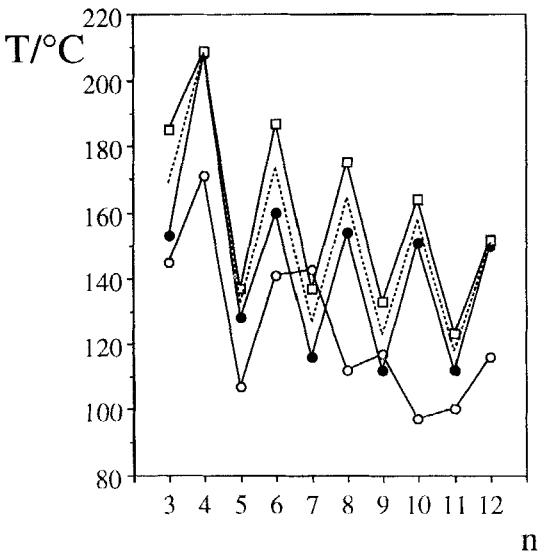

Figure 16. The dependence of the melting points on the length of the flexible alkyl spacer for the CB.O*n*O.2 series indicated by ○, the BCBO*n* series denoted by □ and the 2.O*n*O.2 series represented by ●. The broken line joins the mean values of the melting points for the symmetric dimers.

Downloaded At: 10:48 26 January 2011

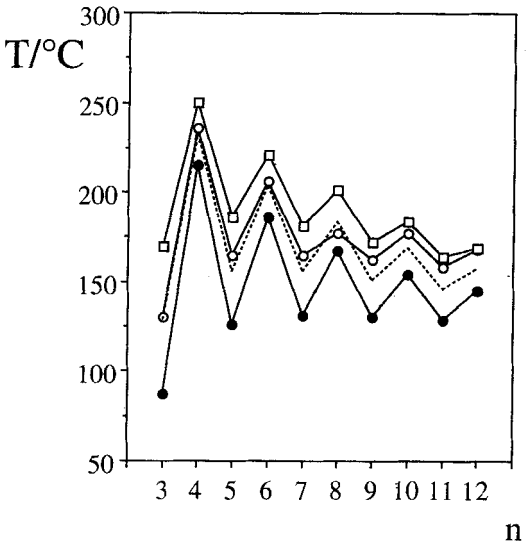

Figure 17. The dependence of the nematic–isotropic transition temperatures on the length of the flexible alkyl spacer for the CB.O*n*O.2 series indicated by ○, the BCBO*n* series denoted by □ and the 2.O*n*O.2 series represented by ●. The broken line joins the mean values of the clearing points for the symmetric dimers.

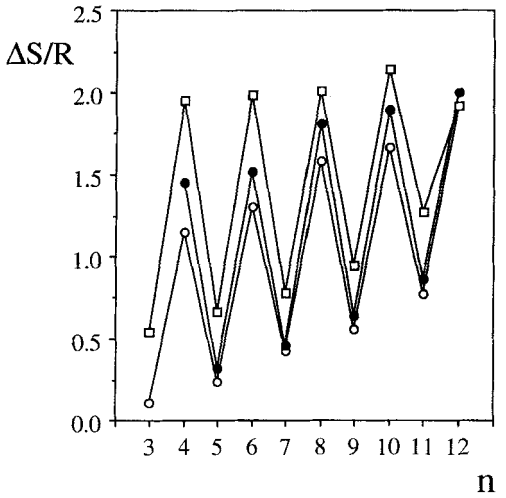

Figure 18. The dependence of the nematic–isotropic transitional entropies on the length of the flexible alkyl spacer for the CB.O*n*O.2 series indicated by ○, the BCBO*n* series denoted by □ and the 2.O*n*O.2 series represented by ●.

Downloaded At: 10:48 26 January 2011

crystals and a molecular field theory has suggested recently that this should be interpreted in terms of the alternation in the long range orientational order [9]. This view is supported by the observation of a large alternation for the second rank order parameter for the *para*-axis of the cyanobiphenylyl group of the α,ω-bis(4-cyanobiphenyl-4′-yloxy)alkanes [22]. Figure 18 also shows the entropies associated with the nematic–isotropic transition for the two symmetric series and for any given homologue the entropy of transition increases in the order,

$$\text{BCBO}n(\square) > 2.\text{O}n\text{O}.2(\bullet) > \text{CB}.\text{O}n\text{O}.2(\circ).$$

The sole exception to this is BCBO12 which exhibits a $\Delta S_{NI}/R$ slightly lower than that of 2.O12O.2. This general trend is slightly surprising as it might be expected that a specific interaction would give rise to larger transitional entropies and is not in accord with a previous observation that some non-symmetric dimers containing an azobenzene-based mesogenic unit exhibit intermediate values of $\Delta S_{NI}/R$ compared with the parent dimers [4]. However, in that case we might have expected the *cis-trans* problem of substituted azobenzenes to have spoilt the intermediate behaviour. Specifically, the *cis*-isomer of an azobenzene is considerably more biaxial than the *trans*-isomer and thus, the thermal interconversion of *trans* to *cis* acts to reduce not only the clearing temperature, but also the clearing entropy. This effect would be greater for symmetric dimers containing two azobenzene units than for non-symmetric dimers containing just a single azobenzene moiety. Therefore, $\Delta S_{NI}/R$ for the non-symmetric dimers would be anticipated to be greater than the symmetric dimers comprising azobenzene moieties, but less than that for the other symmetric series.

Downloaded At: 10:48 26 January 2011

3.2.2. *CBO.nO.6 series*

The transitional properties of this series are given in table 3; all ten homologues are liquid crystalline. In order to reveal the smectic behaviour for the propyl and pentyl members the samples required rapid cooling and the formation of the smectic texture was accompanied by the onset of crystallization preventing a thorough examination of the optical textures. In consequence, these phases are only tentatively assigned as smectic A phases. The dependence of the transition temperatures on the length of the flexible alkyl spacer is shown in figure 19 and immediately apparent is the dramatic

Table 3. The transition temperatures of the CB.O*n*O.6 series; ( ) denotes a monotropic transition. The smectic phases exhibited by compounds with $n=6$ or $n \geqslant 8$ have intercalated structures.

n	T_{C-}/°C	T_{JS_I}/°C	$T_{S_IS_C}$/°C	T_{BS_A}/°C $T_{S_CS_A}$/°C†	T_{S_AN}/°C	T_{NI}/°C T_{S_AI}/°C‡
3	111				(45)	117
4	116					217
5	100				(67)	149
6	116			(84)	(105)	195
7	109			(73)	(78)	150
8	135			(126)	166	190
9	81	(62)	83	112†	118	149
10	112			(111)	165	168
11	93	(60)	(86)	112†	138	147
12	111			114		165‡

Table 4. The smectic A_c periodicity, d, and the estimated all-*trans* molecular length, l, for the CB.O*n*O.6 series.

n	T/T_{SAN}	d/Å	l/Å	d/l
6	0·98	19·1	38·8	0·49
8	0·99	20·0	41·5	0·48
9	0·99	20·6	41·8	0·49
10	0·98	22·1	43·7	0·50
11	0·98	22·3	44·0	0·50
12	0·99	23·5	46·2	0·50

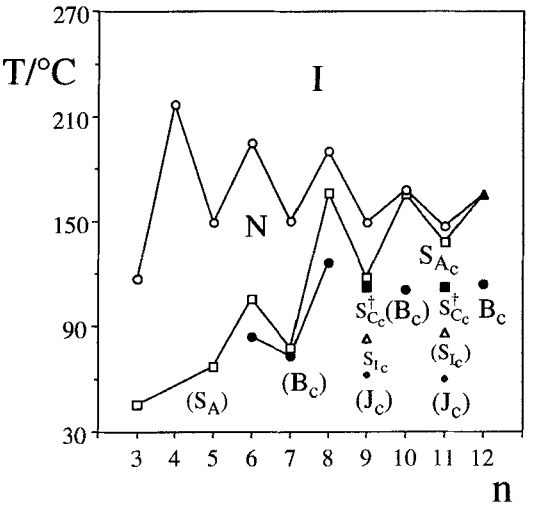

Figure 19. The dependence of the transition temperatures on the number of methylene groups, n, in the flexible alkyl spacer for the CB.O*n*O.6 series. The nematic–isotropic transition is denoted by ○, ▲ indicates the smectic A–isotropic transition, □ the smectic A–nematic transition, ● the crystal B–smectic A transition, ■ the smectic C–smectic A transition, △ the smectic I–smectic C transition and ◇ the crystal J–smectic I transition. The melting points have been omitted for the sake of clarity.

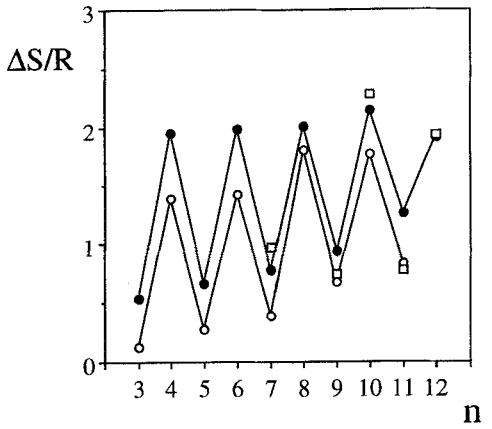

Figure 20. The dependence of the nematic–isotropic transitional entropies on the length of the flexible alkyl spacer for the CB.O*n*O.6 series indicated by ○, the BCBO*n* series denoted by ● and the 6.O*n*O.6 series represented by □.

Downloaded At: 10:48 26 January 2011

alternation of both the clearing temperatures and the smectic A–nematic transition temperatures. The thermal stability of the smectic A phase increases with n as was observed for the CB.O*n*O.2 series. A pronounced odd–even effect is also seen in the entropy of transition associated with the nematic–isotropic transition as shown in figure 20 together with the results for the symmetric dimers; such behaviour has been rationalized in the preceding section. Table 4 gives the layer spacings, d, in the smectic A phases together with the estimated molecular lengths, l, and the d/l ratio in each case is approximately 0·5, again indicating an intercalated structure as described for the CB.O*n*O.2 series. The smectic phases exhibited by the propyl, pentyl and heptyl homologues tended to crystallize during the X-ray diffraction experiment and so the layer spacings are not available for these compounds.

The determination of the stacking sequences in the crystal B_e phases exhibited by the CB.O*n*O.6 series was carried out using X-ray diffraction of aligned samples and by applying the arguments offered for the CB.O*n*O.2 series. Thus the sixth, eighth, tenth and twelfth homologues exhibit a crystal B_e phase having an ABCA packing sequence. On cooling CB.O9O.6 from the intercalated S_C phase into the smectic I_e phase, the wide angle region in the X-ray diffraction pattern of an unaligned sample narrows, reflecting an increase in the molecular translational ordering within the smectic layer. Figure 21 shows the X-ray diffraction pattern for an aligned sample and three bars of diffuse scattering are evident in the wide angle region characteristic of a smectic I phase [23]. On further cooling, the diffuse scattering in the wide angle region sharpens into a series of Bragg peaks implying a transition into a crystal smectic phase. Figure 22 shows the X-ray diffraction pattern for an aligned sample of this phase and this is characteristic of a crystal J phase. Thus, we have unambiguously identified the first examples of the intercalated smectic I and crystal J phases.

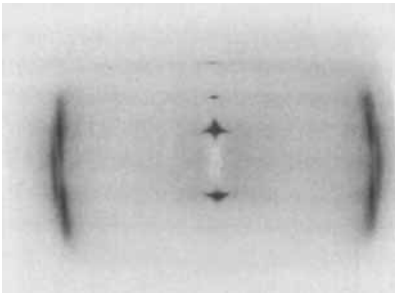

Figure 21. The X-ray diffraction pattern for an aligned sample of the smectic I_e phase of CB.O9O.6 at 65°C.

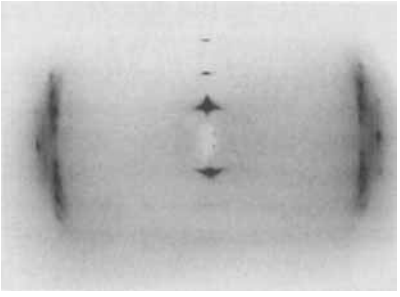

Figure 22. The X-ray diffraction pattern for an aligned sample of the crystal J_e phase of CB.O9O.6 at 60°C.

Downloaded At: 10:48 26 January 2011

The layer spacing for the smectic phases of CB.O9O.6 varies by less than 0·4 Å over the whole temperature range. This is of comparable magnitude to the experimental error and hence, it is not possible to draw any firm conclusions from these data concerning the temperature dependence of the layer spacing. However, it does suggest, as we have already noted, that the intercalated structure of the smectic A phase is preserved in the higher ordered smectic phases. On entering the intercalated smectic C phase, the layer spacing begins to fall, although the total decrease in d over the whole range of the phase is just 0·3 Å. On passing through the smectic I_c phase the layer spacing increases by slightly less than 0·3 Å and is essentially constant in the crystal J_c phase. The apparently paradoxical lack of decrease in the layer spacing for the smectic I_c phase is presumably a result of the competition between the increase in the tilt angle order parameter, which tends to lower the spacing, and the increase in the orientational and translational order at the transition which increases the layer spacing. Alternatively, if we consider the model to be proposed later to describe the S_{C_c}–A_{A_c} transition, then at the S_{C_c}–S_{A_c} and the S_{I_c}–S_{C_c} transitions a change in the layer spacing would not be anticipated. This situation arises because at these transitions only the tilt angle direction distribution function changes, and this will not affect the layer spacing.

The melting points of the CB.O*n*O.6 series are compared to those of the BCBO*n* and 6.O*n*O.6 series in figure 23 and the behaviour is similar to that observed in figure 16 for the CB.O*n*O.2 series, although the dependence of the melting points on n for the CB.O*n*O.6 series is more regular. Again the non-symmetric dimers tend to have the lowest melting points of the series and, therefore, exhibit a considerable negative deviation from the mean of the values for the symmetric dimers. This may be likened to the eutectic behaviour exhibited by mixtures of like dimers which we shall discuss later. Figure 24 compares the clearing temperatures of the three series and, as for the CB.O*n*O.2 series, the clearing temperatures of the CB.O*n*O.6 series are intermediate

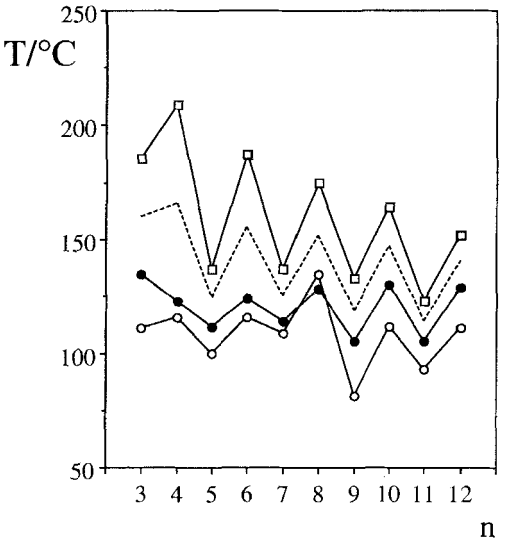

Figure 23. The dependence of the melting points on the length of the flexible alkyl spacer for the CB.O*n*O.6 series indicated by ○, the BCBO*n* series denoted by □ and the 6.O*n*O.6 series represented by ●. The broken line joins the mean values of the melting points for the symmetric dimers.

Downloaded At: 10:48 26 January 2011

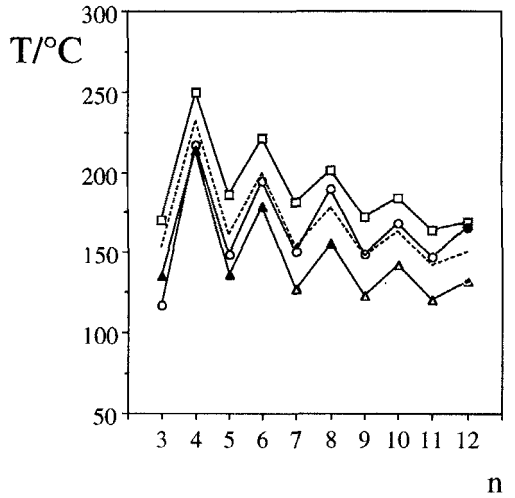

Figure 24. The dependence of the clearing temperatures on the length of the flexible alkyl spacer for the CB.O*n*O.6 series indicated by ● ○, the BCBO*n* series denoted by □ and the 6.O*n*O.6 series represented by ▲ △. Open symbols represent nematic–isotropic transitions, while closed symbols denote smectic–isotropic transitions. The broken line joins the mean values of the clearing points for the symmetric dimers.

Downloaded At: 10:48 26 January 2011

between those of the symmetric dimers. In contrast to the behaviour observed for the CB.O*n*O.2 series, however, the CB.O*n*O.6 series exhibits a relatively small negative deviation away from the mean values of the clearing temperatures of the symmetric dimers for $n = 3$–7 and a positive deviation for the remaining homologues. We should note that we are not comparing like transitions in all cases; the BCBO*n* series exhibits exclusively nematic behaviour, with the exception of CB.O10O.6, the CB.O*n*O.6 series also shows nematic–isotropic transitions, while $n = 3$–6 and 8 of the 6.O*n*O.6 series exhibit smectic A–isotropic transitions.

Figure 20 shows also the nematic–isotropic entropies exhibited by the BCBO*n* (●) and 6.O*n*O.6 (□) series and as we have already seen for the CB.O*n*O.2 series, the values of $\Delta S_{NI}/R$ shown by the non-symmetric dimers (○) tend to be lower than those of either symmetric series. It is interesting to note that for even members of the 6.O*n*O.6 series, $\Delta S_{NI}/R$ is greater than for the corresponding BCBO*n* member, whereas for odd members this is reversed. Thus there is an increase in the magnitude of the alternation in $\Delta S_{NI}/R$ on increasing the length of the terminal alkyl chain from the 2.O*n*O.2 to the 6.O*n*O.6 series. This may reflect the increased biaxiality of the odd members of the 6.O*n*O.6 series as compared with the analogous 2.O*n*O.2 compounds, while for even members the increase in $\Delta S_{NI}/R$ on increasing the length of the terminal alkyl chain suggests an increase in the conformational contribution to the entropy of transition.

3.2.3. *CB.OnO.10 series*

The transitional properties of the CB.O*n*O.10 series are given in table 5. All ten members of this series exhibit liquid crystalline behaviour. Figure 25 shows the dependence of the transition temperatures on the number of methylene units in the flexible core and again the clearing temperatures show a dramatic alternation which attenuates quite rapidly on increasing *n*. In contrast, the large alternation exhibited by the nematic–isotropic entropies, see figure 26, does not attenuate on increasing the

Table 5. The transition temperature of the CB.O*n*O.10 series; ( ) denotes a monotropic transition.

n	T_{C-}/°C	$T_{S_{Cd}S_{Ad}}$/°C $T_{S^{\dagger}_{C_c}S_{A_c}}$/°C‡	$T_{S_{Ad}N}$/°C $T_{S_{A_c}N}$/°C§	$T_{S_{Ad}}I$/°C¶ T_{NI}/°C
3	91	(87)		115¶
4	112	134		199¶
5	101	(87)	106	137
6	118	(107)	155	180
7	114	87	90	138
8	117			164
9	92			137
10	118		126§	154
11	100	(86)‡	108§	135
12	117		146§	148

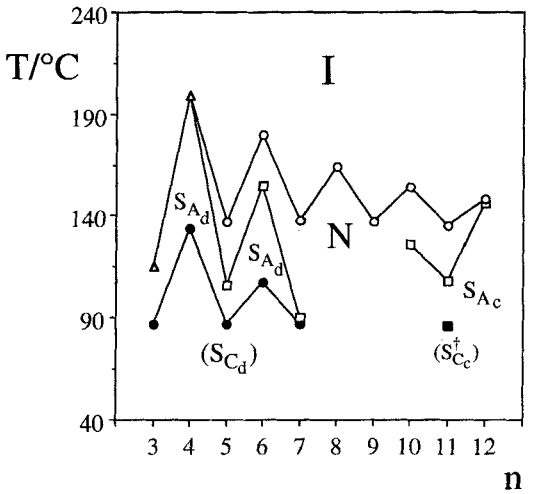

Figure 25. The dependence of the transition temperatures on the number of methylene groups, *n*, in the flexible alkyl spacer for the CB.O*n*O.10 series. The nematic–isotropic transition is denoted by ○, △ indicates the smectic A–isotropic transition, □ the smectic A–nematic transition, ● the smectic C_d–smectic A transition and ■ the alternating smectic S_{C_c}–smectic A transition. The melting points have been omitted for the sake of clarity.

length of the spacer. The nematic–isotropic entropies for the non-symmetric dimers tend to be lower than those of the BCBO*n* series. In contrast to this largely anticipated behaviour, however, the thermal stability of the smectic A phase is very unusual. CB.O3O.10 and CB.O4O.10 exhibit smectic A–isotropic transitions, while the fifth, sixth and seventh homologous show a smectic A–nematic transition. The thermal stability of the smectic A phase, either T_{S_AN} or T_{S_AI}, exhibits a very pronounced odd–even effect and the underlying trend in the temperatures over these five homologues is a decreasing one. Indeed, the stability of the smectic phase decreases to such an extent that the eighth and ninth members are solely nematogenic. Surprisingly, smectic properties re-emerge subsequently with the decyl homologue and there is an increasing trend in the thermal stability of the phase over the final three homologues. Table 6 gives the layer spacings, *d*, in the smectic phase and compares them with the estimated

Downloaded At: 10:48 26 January 2011

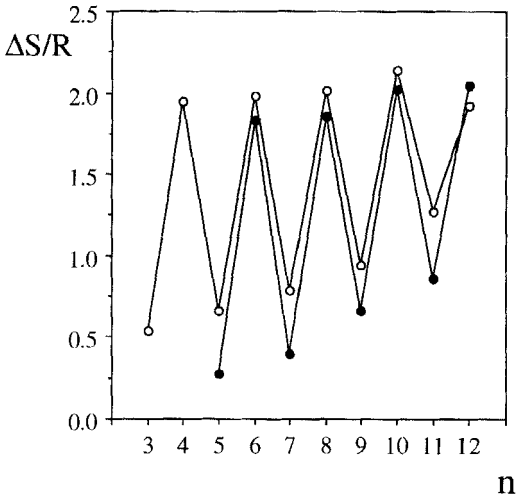

Figure 26. The dependence of the nematic–isotropic transitional entropies on the length of the flexible alkyl spacer for the CB.O*n*O.10 series represented by ● and for the BCBO*n* series denoted by ○.

Downloaded At: 10:48 26 January 2011

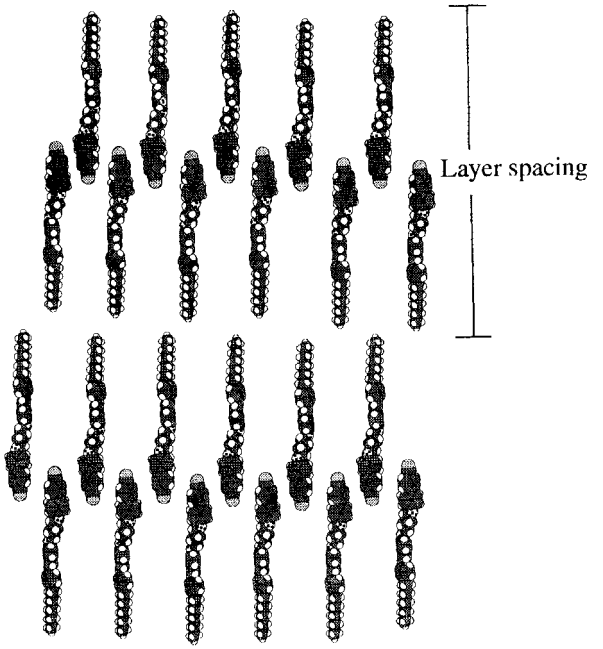

Figure 27. A sketch of the interdigitated smectic A phase.

Table 6. The smectic A periodicity, *d*, and the estimated all-*trans* molecular length, *l*, for the CB.O*n*O.10 series.

n	T/T_{S_AN} T/T_{S_AI}†	*d*/Å	*l*/Å	*d*/*l*
3	0·98†	65·4	38·6	1·7
4	0·97†	74·0	41·4	1·8
6	0·97	77·8	43·6	1·8
7	0·99	84·5	44·2	1·9
10	0·98	24·2	48·6	0·5
11	0·98	24·4	49·8	0·5
12	0·99	25·4	51·0	0·5

molecular lengths, *l*. It is clear that the structure of the smectic phases exhibited by the early members for which *d*/*l* is approximately 1·8 differs from that exhibited by the tenth, eleventh and twelfth homologues for which *d*/*l* is approximately 0·5. The *d*/*l* ratio of 1·8 suggests an interdigitated structure in which the like parts of the molecule overlap and this is sketched in figure 27. The driving force of this structure is, presumably, the electrostatic interaction between the polar and polarizable cyanobiphenylyl groups, while the smectic phase results from the molecular inhomogeneity produced by the long terminal alkyl chains. Space is filled in this structure presumably via the flexibility of the decyl chain. It should be noted also that the length of the terminal chains prohibits the formation of an intercalated structure for the space between the layers, governed by the length of the flexible core, could not accommodate the long terminal chains. The phase structure for the higher homologues is an intercalated one sketched in figure 11 and is driven by the mixed mesogenic unit–mesogenic unit interaction. Thus, the structure of the smectic A phase formed by the non-symmetric dimers depends on the relative lengths of the spacer and terminal chain. The disappearance of smectic behaviour for intermediate chain lengths is presumably the result of a competition between the two incompatible structures, neither of which wins, and hence, the nematic phase is observed. Similar behaviour was reported for the CB.O6O.*m* series in which the terminal chain length was varied [3].

Figure 28 shows the temperature dependence of the layer spacing in the smectic C_d and A_d phases exhibited by CB.O4O.10. The dependence of the layer spacing on temperature is consistent with a second order transition and this is supported by differential scanning calorimety. On decreasing the temperature, the layer spacing measured in the smectic A_d phase increases and this reflects, in part, a damping of the molecular orientational thermal fluctuations and an increase in the conformational order. At the transition to the smectic C_d phase, the layer spacing decreases and this continues throughout the temperature range of the phase. This results from the tilting of the director with respect to the layer normal and subsquent growth of the tilt angle with decreasing temperature. It is important to note that the interdigitated structure of the smectic A phase is preserved in the smectic C phase. If we compare this with the behaviour of CB.O9O.6 described earlier, it is immediately apparent that the layer spacing for CB.O4O.10 is far more temperature sensitive than that of CB.O9O.6. In consequence, the global tilt angles of the tilted phases exhibited by CB.O4O.10 are considerably greater than those shown by CB.O9O.6. This suggests that the greatly preferred orientation for even membered dimers in the intercalated structure is an

Downloaded At: 10:48 26 January 2011

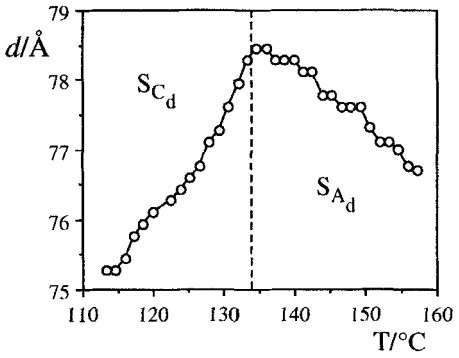

Figure 28. The temperature dependence of the layer spacing in the smectic C and A phases of CB.O4O.10.

orthogonal one. Indeed, the only compounds to exhibit tilted intercalated phases are CB.O9O.2, CB.O9O.11, CB.O9O.6, CB.O11O.6 and CB.O11O.10. It is important to note that these all possess long odd membered spacers and it is envisaged that such bent molecules experience great difficulties in packing efficiently into the intercalated network.

A new structural modification of the smectic C phase was found to be exhibited by certain semi-flexible main-chain liquid crystal polymers [24]. In this variant, the mesogenic units are tilted with respect to the layer normals as in the conventional smectic C phase, but the tilt direction alternates in passing from one layer to the next; this is shown schematically in figure 29 (*a*). The structure of this phase is very similar to that of the antiferroelectric chiral smectic C phase, see figure 29 (*b*), and has been denoted the S_{C_2} phase. This modification has also been observed for the dimeric liquid crystal [14, 15],

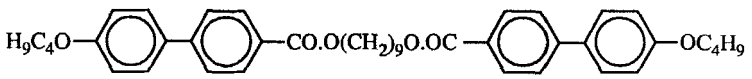

A characteristic feature of the S_{C_2} phase is the observation of both types of point singularity in the schlieren optical texture [14, 25]. This suggests that the S_C phase formed on cooling an intercalated smectic A structure may be the intercalated analogue (see figure 29 (*c*)) of an antiferroelectric S_C phase, but only from the standpoint of the alternating tilt. The common factor linking the three phase structures shown in figure 29 is that the tilt direction alternates between adjacent layers. The requirement for the observation of such an alternation in the sense of the tilt angle is simply a correlation of the mesogenic groups. For the polymer this is provided by the flexible spacer and the polymeric nature of the system. For the antiferroelectric phase, it is provided through dipolar forces between the chiral monomers, while for our non-symmetric dimers the correlation originates from the specific interaction between the unlike mesogenic groups. The strong similarity between these three structures, therefore, demands that a single label should be used to describe them. Since all these structures are examples of alternating smectic C phases, we propose the use of † to designate this structural feature. Thus, the intercalated alternating smectic C phase would be referred to as $S_{C_c}^{\dagger}$ while the antiferroelectric smectic C phase would be denoted $S_C^{\dagger *}$. A possible model with which to describe the $S_{C_c}^{\dagger}$–S_{A_c} transition invokes the freezing of the precessional rotation of the molecules about their long axes resulting in a long range correlation of the tilt angle. Such a model, first proposed by Wulf to account for the S_A–S_C transition

Downloaded At: 10:48 26 January 2011

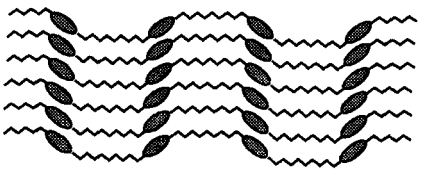

(*a*)

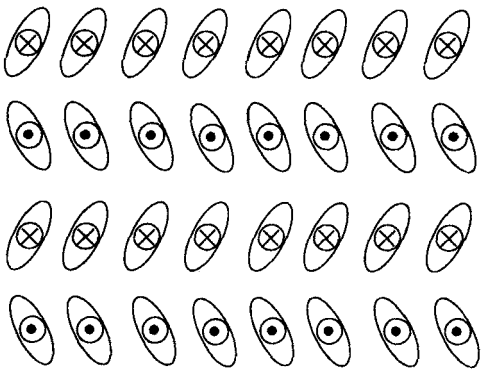

(*b*)

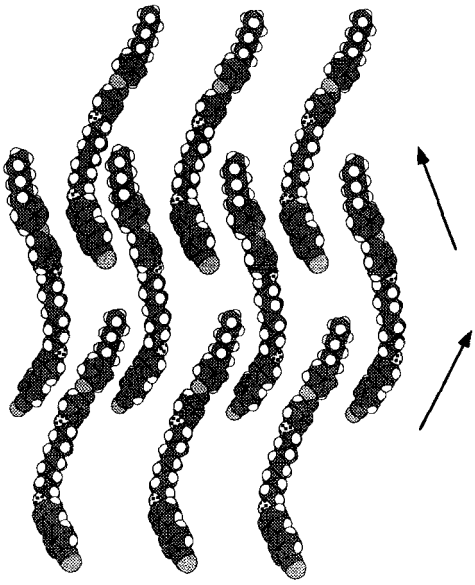

(*c*)

Figure 29. Sketches of the molecular organization in (*a*) the S_{C_2} phase for semi-flexible main-chain liquid crystal polymers, (*b*) in the antiferroelectric smectic C phase and (*c*) in the intercalated smectic C phase exhibited by non-symmetric dimeric liquid crystals containing odd-membered spacers.

Downloaded At: 10:48 26 January 2011

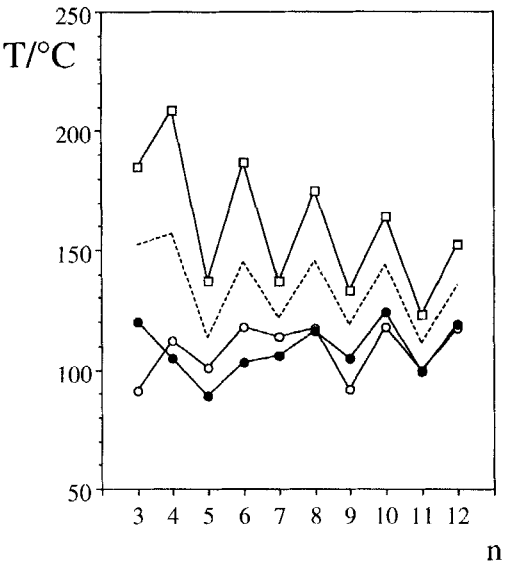

Figure 30. The dependence of the melting points on the length of the flexible alkyl spacer for the CB.O*n*O.10 series indicated by ○, the BCBO*n* series denoted by □ and the 10.O*n*O.10 series represented by ●. The broken line joins the mean values of the melting points for the symmetric dimers.

Downloaded At: 10:48 26 January 2011

in conventional mesogens [26] for which the molecules are tilted with respect to the layer normals in both phases, successfully predicts the absence of a large change in the layer spacing at the transition. Thus in the $S_{C_c}^{\dagger}$ phase the global tilt angle is zero but locally, within a layer, is non-zero.

Figure 30 compares the melting points of the CB.O*n*O.10 series with those of the analogous symmetric dimers and as we have seen for the other two non-symmetric series, the melting points are significantly lower than the mean values, although for this series the melting points for the non-symmetric materials are in several instances slightly higher than those of the 10.O*n*O.10 series. The clearing temperatures for the three series, as well as the calculated mean values for the symmetric dimers are shown in figure 31. Again the BCBO*n* series (□) exhibits the highest clearing temperatures, but for small values of *n* the transition temperatures of the 10.O*n*O.10 series (▲) are greater than those of the non-symmetric dimers (○ ●). Indeed, even though the transition temperatures of the non-symmetric series become greater than those of the 10.O*n*O.10 series as *n* is increased, they are still less than the mean values of the symmetric dimers. We should stress, however, that these comparisons are between unlike transitions.

We have now seen three types of behaviour when we compare the clearing temperatures of the non-symmetric dimers with those of the parent symmetric dimers. It should be stressed that the nature of the clearing transition varies and hence, in some instances we are comparing unlike transitions. However, for the majority of liquid crystal series, the smectic–isotropic transition temperatures can be obtained from an extrapolation of the nematic-isotropic transition temperatures (see figure 24). We believe that this justifies the comparisons of the clearing temperatures. In order to investigate the relative magnitudes of the deviations that we have noted for the clearing

temperatures of the non-symmetric dimers T_{AB} from the mean of those for the symmetric dimers (T_A and T_B), we define a scaled deviation as,

$$\Delta T_{SC} = \frac{2T_{AB} - (T_A + T_B)}{(T_A + T_B)}.$$

Figure 32 shows the dependence of ΔT_{SC} on n for each of the three non-symmetric dimer series. This reveals that the relative magnitude of these effects is typically very small and the general trend is for ΔT_{SC} to become less negative with increasing n. For the CB.OnO.2 series, ΔT_{SC} is small, less than 5 per cent, and positive with the exception of CB.O8O.2 for which ΔT_{SC} is small but negative. For the CB.OnO.6 series, ΔT_{SC} is initially negative but as n increases becomes positive. Finally, for the CB.OnO.10 series, ΔT_{SC} is negative for all values of n, but becomes less negative as n increases. Thus,

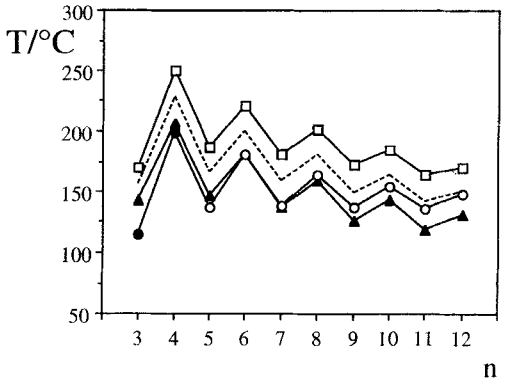

Figure 31. The dependence of the clearing temperatures on the length of the flexible alkyl spacer for the CB.OnO.10 series indicated by ○ ●, the BCBOn series denoted by □ and the 10.OnO.10 series represented by ▲. Open symbols represent nematic–isotropic transitions, while closed symbols denote smectic–isotropic transitions. The broken line joins the mean values of the clearing points for the symmetric dimers.

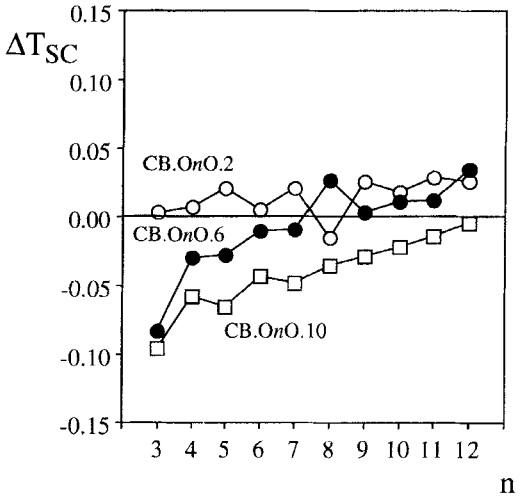

Figure 32. The dependence of ΔT_{SC} on the length of the flexible alkyl spacer for the CB.OnO.m series.

Downloaded At: 10:48 26 January 2011

increasing n results in ΔT_{SC} becoming less negative and this is most marked for the CB.OnO.6 and CB.OnO.10 series. By comparison the increase for the CB.OnO.2 series on increasing n is considerably smaller. If we consider this in terms of ideal behaviour, i.e., $\Delta T_{SC}=0$, then on increasing n for the CB.OnO.10 series, the behaviour becomes more ideal, whereas for the CB.OnO.2 series, it becomes less ideal and for the CB.OnO.6 series, initially it becomes more ideal and then less ideal.

To begin to understand such behaviour, at least qualitatively, we should first consider the case of an ideal binary mixture of nematogens for which $\Delta T_{SC}=0$ and then we will treat deviations from this. Within the framework of a molecular field theory developed to predict phase diagrams for binary mixtures of nematogens, three intermolecular energy parameters, ε_{AA}, ε_{BB} and the mixed parameter ε_{AB}, must be defined [27]. The parameters ε_{AA} and ε_{BB} for the interactions between like species are proportional to the nematic–isotropic transition temperatures of the pure nematogens. If ε_{AB}, the interaction parameter for unlike species, is assumed to be the geometric mean of ε_{AA} and ε_{BB}, then the transition temperature of the mixture is simply the weighted average of those of the components, i.e. a linear dependence of T_{NI} on composition is predicted, in other words $\Delta T_{SC}=0$. Such behaviour is often found experimentally. If we allow for a positive deviation in ε_{AB} from the geometric mean approximation, then a curve lying above the straight line is observed, i.e. $\Delta T_{SC}>0$, whereas a negative deviation in ε_{AB} results in a curve lying below the straight line, i.e. $\Delta T_{SC}<0$. Furthermore, quite small deviations of ε_{AB}, for example, $\pm 1{\cdot}85$ per cent, are readily discernible in the phase diagram as curved phase boundaries [27, 28]. The relatively small values of ΔT_{SC} exhibited by the non-symmetric dimers suggest, therefore, that the deviation from the geometric mean approximation is also small, provided of course the dimers approximate to the rigid, cylindrically symmetric particles assumed in the theory [27].

Downloaded At: 10:48 26 January 2011

It is important to note that the preceding discussion does not refer to the type of mesogenic units in the non-symmetric dimer, nor does it consider the nature of the mixed interaction. It would be reasonable to assume, therefore, that the geometric mean approximation will be violated by all non-symmetric dimers which exhibit a specific interaction between the two unlike mesogenic units. There are just two other complete homologous series of non-symmetric dimers described in the literature with which to test this assumption. The dependence of ΔT_{SC} on n for the NABOnO.4 series [4],

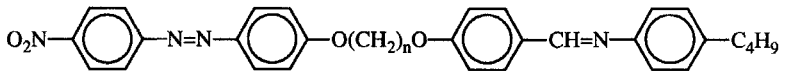

is shown as figure 33. ΔT_{SC} initially is relatively large and negative, becoming more ideal as n is increased. Further increases in n result in ΔT_{SC} adopting small, positive values. The second series with which to test these ideas concerns the α-(4-cyanobiphenyl-4′-yloxy)-ω-(1-pyreniminebenzylidene-4′-oxy)alkanes [8],

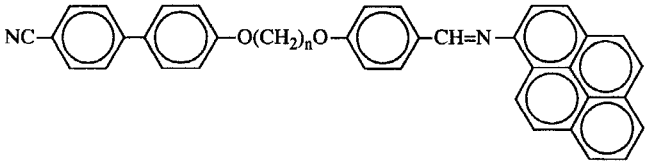

and these can be compared with the BCBOn series and the α,ω-bis(1-pyreniminebenzylidene-4′-oxy)alkanes [29]. This particular series does not contain a terminal alkyl chain and this clearly strengthens the approximation that the molecules

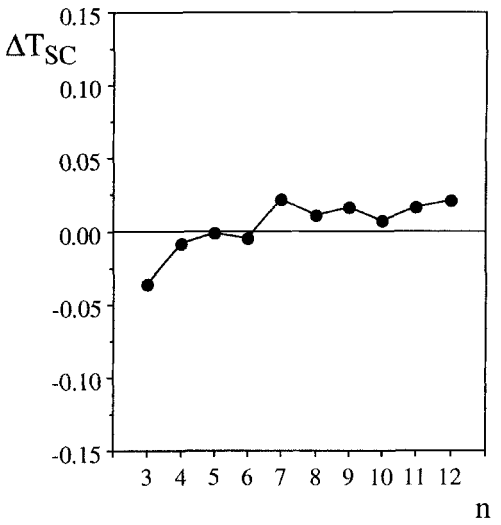

Figure 33. The dependence of ΔT_{SC} on the length of the flexible alkyl spacer for the NABO*n*O.4 series.

Downloaded At: 10:48 26 January 2011

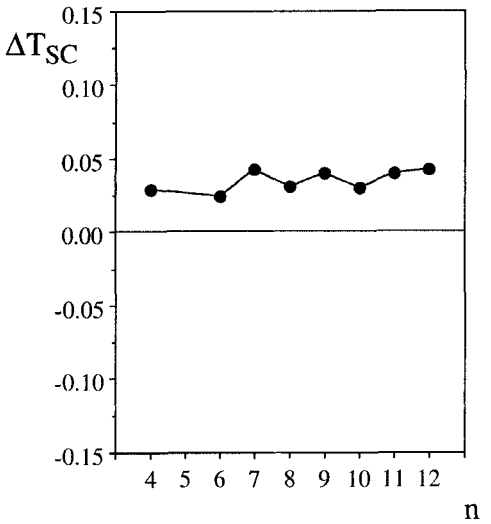

Figure 34. The dependence of ΔT_{SC} on the length of the flexible alkyl spacer for pyrene containing dimers.

are rigid, cylindrically symmetric particles. Figure 34 shows the dependence of ΔT_{SC} on n for these materials and it can be seen that ΔT_{SC} is positive and relatively insensitive to changes in n. It is worth noting also that the small deviation in ΔT_{SC}, approximately 5 per cent, suggests that the deviation of ε_{AB} away from the geometric mean approximation is also small. It appears, therefore, that in the absence of terminal chains or if the chain is short, ΔT_{SC} tends to be small and positive, whereas for long terminal chains the sign and magnitude of ΔT_{SC} is dependent on the m/n ratio. We will return to a more quantitative discussion of ΔT_{SC} for these and other series later.

3.3. *The dependence of the transitional properties on the length of the terminal chains*

Thus far we have considered only the effects of varying the length of the spacer while holding the terminal chain constant. We now turn our attention to the opposite of this, varying the terminal chain while holding the spacer length constant. The three series we have chosen for this investigation, CB.O3O.*m*, CB.O4O.*m* and CB.O5O.*m* together with CB.O6O.*m* [3] allow us to consider the effects of the terminal chain on compounds having both odd and even spacers.

3.3.1. *CB.O3O.*m

The transitional properties of the CB.O3O.*m* series are given in table 7. All eleven members of this series exhibit liquid crystalline behaviour although the first five homologues are monotropic. The smectic phase exhibited by the propyl, butyl, pentyl and hexyl homologues has yet to be identified. The difficulty in doing this arises because of the monotropic nature of the phase which crystallizes rapidly on forming. The dependence of the transition temperatures on the length of the terminal alkyl chain for this series is shown in figure 35. The increase in the nematic–isotropic transition temperature on replacing the *p*-protons by methyl groups is about 24 per cent. In contrast, the increase in the molecular length is considerably smaller; for example, for the spacer in the all-*trans* conformation it is only approximately 4·5 per cent. This seems to be far too small to account for the change in T_{NI}. However, computer simulation studies of the transitional behaviour of hard particles have revealed that as well as the length to breadth ratio, the shape of the object can also have a dramatic influence on the nematic–isotropic transition density. For example, for hard ellipsoids a length to breadth ratio of at least 3 : 1 seems to be essential for the observation of a nematic phase [30, 31], whereas for hard spherocylinders this ratio seems to be of the order of 6 : 1 or greater [32, 33]. Given this strong dependence on shape and the clear influence of repulsive forces on the nematic–isotropic transition [30, 31], it is possible that the dramatic increase in T_{NI} on adding the methyl groups may well result from a change in shape of the mesogenic unit rather than in any significant enhancement of the

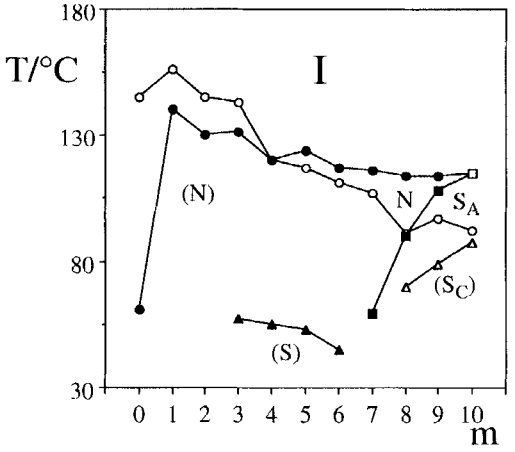

Figure 35. The dependence of the transition temperatures on the length of the terminal alkyl chain for the CB.O3O.*m* series. The melting points are denoted by ○, ● indicates the nematic–isotropic transition, □ the smectic A–isotropic transition, △ the smectic C–smectic A transition, ■ the smectic A–nematic transition and ▲ the smectic–nematic transition.

Downloaded At: 10:48 26 January 2011

shape anisotropy. Subsequent increases in the length of the terminal alkyl chain cause the nematic–isotropic transition to fall with a small alternation between odd and even members of the series in a manner comparable to that observed for conventional monomeric nematics [34, 35] and symmetric dimers [9]. The melting points of this series generally decrease with increasing chain length and all lie below the mean value of those of the corresponding symmetric dimers. The smectic–nematic transition temperatures initially fall before rising as m is increased, although it should be noted that the difference between T_{SN} values for the early members are small and, considering the difficulties associated with their measurement, probably within experimental error. The increase in thermal stability of the smectic phase appears coincident with the formation of interdigitated structures. We have seen already that CB.O3O.10 exhibits a S_{A_d}-isotropic transition and we anticipate that $m = 7$, 8 and 9 also form interdigitated phases.

3.3.2. *CB.O4O.*m

The transitional properties of the CB.O4O.*m* series are listed in table 8 and all eleven homologues are enantiotropic mesogens. Figure 36 shows the dependence of the transition temperatures on the length of the terminal alkyl chain. The melting points tend to decrease with increasing m and, as with the CB.O3O.*m* series, lie below the mean values of the melting points of the corresponding symmetric dimers. The nematic–isotropic transition temperature can be seen to behave in a similar fashion to that observed for the CB.O3O.*m* series. The smectic A–nematic transition temperatures show a very unusual dependence on m. For conventional monomeric [36] as well as symmetric dimeric liquid crystals [9], the smectic A–nematic transition temperature simply increases with increasing chain length. Such an increase is observed for the first three members of the CB.O4O.*m* series but on passing from CB.O4O.2 to CB.O4O.3 there is a dramatic decrease in T_{S_AN} and a further drop in T_{S_AN} is found on passing to CB.O4O.4. This decrease presumably continues as m is increased, for no smectic behaviour is observed for CB.O4O.5, CB.O4O.6 and CB.O4O.7, although their

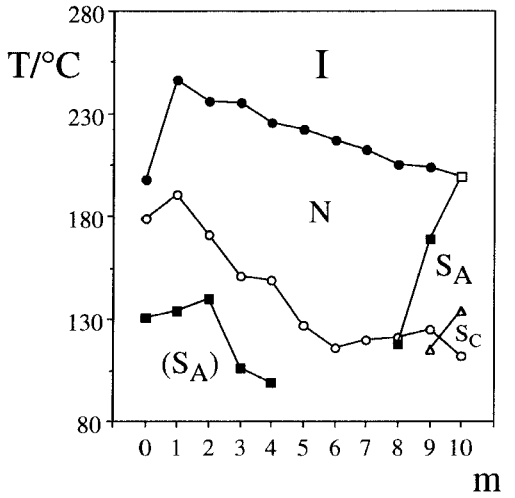

Figure 36. The dependence of the transition temperatures on the length of the terminal alkyl chain for the CB.O4O.*m* series. The melting points are denoted by ○, ● indicates the nematic–isotropic transition, □ the smectic A–isotropic transition, △ the smectic C–smectic A transition and ■ the smectic A–nematic transition.

Downloaded At: 10:48 26 January 2011

Table 7. The transition temperatures of the CB.O3O.*m* series; ( ) denotes a monotropic transition.

m	T_{C-}/°C	$T_{S_CS_A}$/°C	T_{SN}/°C T_{S_AN}/°C†	T_{NI}/°C T_{S_AI}/°C‡
0	145			(61)
1	156			(140)
2	145			(130)
3	143		(57)	(131)
4	120		(55)	(120)
5	117		(53)	(124)
6	111		(45)	117
7	107		(59)†	116
8	91	(70)	(90)†	114
9	97	(79)	108†	114
10	91	(87)		115‡

Table 8. The transition temperatures of the CB.O4O.*m* series; ( ) denotes a monotropic transition.

m	T_{C-}/°C	$T_{S_CS_A}$/°C	T_{S_AN}/°C	T_{NI}/°C T_{S_AI}/°C†
0	179		(131)	198
1	191		(134)	246
2	171		(140)	236
3	151		(106)	235
4	149		(99)	225
5	127			222
6	116			217
7	120			212
8	121		(118)	205
9	125	(115)	169	204
10	112	134		199†

Downloaded At: 10:48 26 January 2011

nematic phases may be supercooled to temperatures in the region of 80°C. The smectic A phase then reappears dramatically with the octyl homologue and T_{S_AN} increases for the final three homologues. Indeed, the decyl homologue actually exhibits a smectic A–isotropic transition. This unusual dependence of T_{S_AN} on the length of a terminal alkyl chain was reported also for the CB.O6O.*m* series and is to our knowledge unique to this class of materials. In the Introduction, we broached the rationalization for this currently rare behaviour and it is very similar to that proposed to explain the behaviour of the CB.O*n*O.10 series, except that for this series the early members exhibited interdigitated phases, while the later members showed intercalated phases. Here the reverse is true with the early members exhibiting intercalated structures while the later members show interdigitated phases. The cross-over from intercalated to interdigitated structures is a result of insufficient space between the layers, which is governed by the length of the spacer in the intercalated modification, to accommodate the terminal chains and so the layers are pushed apart. This reduces the overlap of the aromatic units and hence, also the attractive interactions between the Schiff's base moiety and

the cyanobiphenylyl groups. For long terminal chain lengths, the driving force responsible for the resurgence in smectic behaviour is not this specific interaction. Instead, the electrostatic interaction between the polar and polarizable cyanobiphenylyl groups results in the formation of antiparallel correlations between these moieties and the smectic phase results from the molecular inhomogeneity produced by the long terminal alkyl chains. We should note that the smectic B–nematic transition temperatures for the *trans*-4-(*trans*-4-*n*-alkylcyclohexyl)cyclohexylcarbonitriles [37],

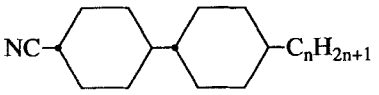

behave initially in a similar manner, in that smectic behaviour is observed for $n = 2$–5, while the heptyl homologue exhibits only a nematic phase. This suggests the presence of strong lateral interactions between the molecules which promote smectic behaviour even for short terminal chain lengths, while packing considerations or the dilution effect of the terminal chain become increasingly important as the chain length is increased.

Downloaded At: 10:48 26 January 2011

3.3.3. *CB.O5O*.m

The transitional properties of the CB.O5O.*m* series are listed in table 9 and all the members exhibit liquid crystalline behaviour, although CB.O5O.0 is a monotropic nematic. Figure 37 shows the dependence of the transition temperatures on *m* and the nematic–isotropic transition temperatures clearly behave in a very similar fashion to that observed for the CB.O3O.*m* and CB.O4O.*m* series. The melting point curve is rather flat and with the exception of CB.O5O.0, all the members exhibit melting points which lie below the mean value of those of the corresponding symmetric dimers suggesting eutectic-like behaviour. The thermal stability of the smectic phase on increasing *m* is unusual because it decreases essentially without alternation from

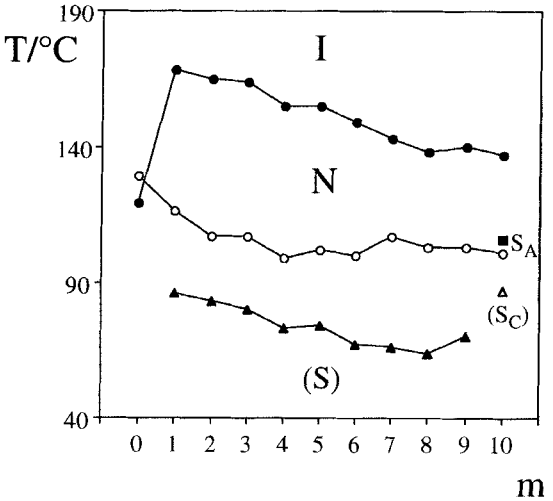

Figure 37. The dependence of the transition temperatures on the length of the terminal alkyl chain for the CB.O5O.*m* series. The melting points are denoted by ○, ● indicates the nematic–isotropic transition, △ the smectic C–smectic A transition, ■ the smectic A–nematic transition and ▲ the smectic–nematic transition.

Table 9. The transition temperatures of the CB.O5O.*m* series; ( ) denotes a monotropic transition.

m	T_{C-}/°C	$T_{S_CS_A}$/°C	T_{SN}/°C T_{S_AN}/°C†	T_{NI}/°C
0	129			(119)
1	116		(86)	168
2	107		(83)	165
3	107		(80)	164
4	99		(73)	155
5	102		(74)	155
6	100		(67)	149
7	107		(66)	143
8	103		(64)	138
9	103		(70)	140
10	101	(87)	106†	137

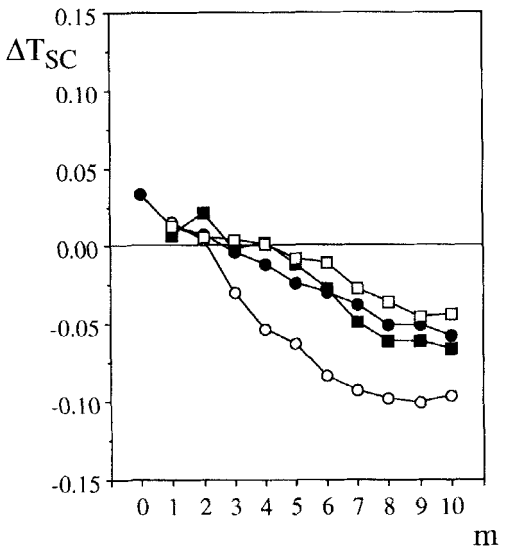

Figure 38. The dependence of ΔT_{SC} on the length of the terminal alkyl chain for the CB.O3O.*m*, ○, the CB.O4O.*m* ●, the CB.O5O.*m* ■, and the CB.O6O.*m* series, □.

CB.O5O.1 to CB.O5O.8 and then rises slightly over the last two homologues. It should be noted that the dependence of T_{S_AN} on *m* is much less dramatic than was observed for the CB.O4O.*m* series and presumably reflects the difficulties encountered in packing bent molecules into the intercalated structure. We should stress, however, that there is no direct evidence that the odd membered compounds of this particular series adopt an intercalated structure and it is impossible to establish this because of the monotropic nature of these phases.

Figure 38 shows the dependence of ΔT_{SC}, i.e. the difference between the clearing temperature of the non-symmetric dimer and the arithmetic mean of that for the symmetric dimers scaled by the latter temperature, on *m* in these series and for the CB.O6O.*m* series [3]. For all four series, ΔT_{SC} for small values of *m* is small and positive,

Downloaded At: 10:48 26 January 2011

but on increasing n becomes large and negative. This is in accord with the earlier observation that the larger the m/n ratio, the more negative ΔT_{SC} becomes. It is possible that our assumption that the nematic–isotropic transition temperatures may essentially be equated to the smectic–isotropic transition temperatures is not valid for large values of m. For example, the 10.OnO.10 series is exclusively smectic [9] and this behaviour is presumably in part the result of the molecular inhomogeneity produced by the long terminal alkyl chains. The virtual nematic–isotropic transition temperatures for the series must lie below the smectic–isotropic transition temperatures. However, if we plot the dependence of the clearing temperature on the length of the terminal alkyl chain, m, for a given value of spacer length n for an m.OnO.m series [9], then it can be seen that the extrapolation we suggest for determining the virtual T_{NI} does appear to be a good one.

The interpretation which we have proposed for the deviation of the clearing temperatures of the non-symmetric dimers from the mean of the corresponding symmetric dimers assumes, in effect, that the constituent molecules are both rigid and cylindrically symmetric. In practice, the presence of the flexible spacer means that the molecules adopt many different conformations most of which have a symmetry lower than cylindrical. It is possible that this behaviour, which is known to influence the transitional properties of the symmetric liquid crystal dimers, may also contribute to the dependence of ΔT_{SC} on the length of the spacer. We have, therefore, calculated ΔT_{SC} using the Marcelja–Luckhurst theory of nematogens composed of flexible molecules in order to explore this possibility [38, 39]. This theory has been described in detail elsewhere and so here we shall only give those details which are necessary to appreciate the significance of the parameters which enter our calculations.

The flexible spacer is assumed to exist in various conformational states as given by the Flory rotameric state theory [40]. The internal energy of each conformer n is

$$U_{int}(n) = N_g E_{tg} + N_{g\pm g\mp} E_{g\pm g\mp}, \tag{1}$$

where N_g is the number of *gauche* links in the spacer and $N_{g\pm g\mp}$ the number of $g\pm g\mp$ sequences. The energy difference between a *gauche* and *trans* link is denoted by E_{tg}, while $E_{g\pm g\mp}$ is the additional energy resulting from a $g\pm g\mp$ sequence. The potential of mean torque for each conformer, which is responsible for their orientational order, is restricted to second rank terms [41]

$$U_{ext}(n, \omega) = -\sum_m X^n_{2m} C^*_{2m}(\omega). \tag{2}$$

Here ω is the orientation of the director in the molecular frame and $C_{2m}(\omega)$ is a second rank spherical harmonic. The interaction strength tensor varies with the conformational state, but can be calculated for each conformer by assuming that it is made up of a tensorial sum of segmental contributions [38, 39]. For the dimer, the segments are taken to be the two mesogenic units and the C–C bonds in the flexible spacer; in addition the oxygen in the ether link is taken to be equivalent to a carbon atom. The segmental units are assumed to have cylindrically symmetric strength tensors with non-zero components X_A and X_B for the two mesogenic groups and X_c for the C–C bonds. The interaction tensor is then

$$X^n_{2m} = X_A C_{2m}(\omega^n_A) + X_B C_{2m}(\omega^n_B) + X_c \sum_j C_{2m}(\omega^n_j), \tag{3}$$

where ω^n_j denotes the orientation of the jth segment in the molecular frame for the nth conformer and the summation is over the C–C and O–C segments in the flexible spacer.

Downloaded At: 10:48 26 January 2011

The nematic–isotropic transition temperature is determined by locating the point at which the difference in the Helmholtz free energy between the isotropic and nematic phases vanishes. This molar free energy difference is

$$A_N - A_I = N_A\{X_A\langle \bar{P}_2^A\rangle + X_B\langle \bar{P}_2^B\rangle + X_c\langle \bar{P}_2^c\rangle\} - RT\ln Z_N/Z_I; \tag{4}$$

here the angular brackets indicate a conformational average over the segmental order parameters, $\bar{P}_2^A$ for the mesogenic group A, $\bar{P}_2^B$ for the other mesogenic group B and $\bar{P}_2^c$ is a sum over the order parameters for each C–C and O–C bond in the spacer. The single particle partition functions are denoted by Z; in the isotropic phase

$$Z_I = 4\pi \sum \exp\{-U_{int}(n)/RT\} \tag{5}$$

and for the nematic phase

$$Z_N = \sum \exp\{-U_{int}(n)/RT\}Q_n. \tag{6}$$

Here Q_n is the orientational partition function

$$Q_n = \int \exp\{-U_{ext}(n,\omega)/RT\}\,d\omega, \tag{7}$$

for the nth conformer.

The determination of the free energy difference requires a knowledge of the three strength parameters X_A, X_B and X_c and in particular how they vary with temperature. These parameters are determined by, amongst other things, the extent of the orientational order. To a first approximation it is assumed that they are linear in the segmental second rank order parameters [38, 39]; for example,

$$N_A X_A = (\varepsilon_{AA}\bar{P}_2^A + \varepsilon_{AB}\bar{P}_2^B + \varepsilon_{Ac}\bar{P}_2^c)/V_m. \tag{8}$$

Here the proportionality constants are related to the anisotropic interactions between the various molecular segments; thus ε_{AA} is a measure of the average interaction between like segments of type A while ε_{AB} is related to the interactions between segment A of one molecule and segments B of the neighbouring molecules. These parameters are taken to be independent of temperature, at least at constant volume. The growth in the molecular size reduces the opportunity for molecular interactions, and this dilution effect is introduced into the theory by the molar volume V_m in the denominator. For the non-symmetric dimers, there are six interaction parameters ε_{AA}, ε_{BB}, ε_{cc}, ε_{AB}, ε_{Ac}, and ε_{Bc} which occur in the theory. In order to reduce this number, the mixed interactions are related to the pure terms by invoking the geometric mean approximation [27], for example,

$$\varepsilon_{AB} = (\varepsilon_{AA}\varepsilon_{BB})^{1/2}. \tag{9}$$

This approximation has an additional, major advantage in that the computational effort in evaluating the free energy is considerably reduced because strength ratios, such as X_B/X_A and X_c/X_A, are predicted to be independent of the orientational order and hence of temperature. They are directly related to the interaction parameters:

$$X_B/X_A = (\varepsilon_{BB}/\varepsilon_{AA})^{1/2} \tag{10}$$

and

$$X_c/X_A = (\varepsilon_{cc}/\varepsilon_{AA})^{1/2}. \tag{11}$$

Downloaded At: 10:48 26 January 2011

Finally in the theory, it is assumed that the parameters needed to describe the behaviour of the symmetric dimers ε_{AA}, ε_{BB}, and ε_{cc} are transferable to the non-symmetric dimers.

The theory clearly contains a variety of adjustable parameters, but some of these are available from other studies. Thus the molar volume is calculated from the tabulations of segmental contributions given by Bondi [42]. The value of E_{tg}(CCCC) for a fragment containing four carbon atoms is assumed to be independent of the position of the fragment in the spacer. However, we have adopted a different value E_{tg}(COCC) for torsional motion about the O–C bond in the spacer. The values employed for these two energy differences are 3·8 kJ mol^{-1} for E_{tg} (CCCC) and 4·8 kJ mol^{-1} for E_{tg} (COCC). The values were obtained by fitting the theory to the order parameter profiles for the chains in the 4-*n*-alkyloxy-4′-cyanobiphenyls [43]; they are also in agreement with determinations of these energies using other techniques. The conformational energy difference $E_{g\pm g\mp}$ was taken to be independent of the location of the $g\pm g\mp$ sequence in the chain and of the atoms in the sequence. The ratio $E_{g\pm g\mp}/E_{tg}$(CCCC) was set equal to 4. In the calculations E_{tg} (CCCC) appears in the Boltzmann factor as E_{tg} (CCCC)/RT. For previous calculations, the value assigned to T was about 320 K and kept fixed so that E_{tg} (CCCC)/RT was set at 1·0. This is, however, unrealistic because the transition temperatures of the dimers vary considerably and this influences the conformational distribution. To overcome this problem, we have set T, in the Boltzmann factor for the internal energy, $U_{int}(n)$, equal to the true transition temperatures for the dimers in the homologous series which we are studying. Such an assumption should not influence the results of the calculations to any significant extent and has the advantage of avoiding an iterative self-consistent calculation. The molecular geometry adopted for the flexible spacer has the CCC bond angle as 113·5° and the torsional angle in the *gauche* conformation as $\pm 112°$. The angle between the assumed symmetry axis of a mesogenic group and the O–C bond in the chain was set at 123·4°. All of these angles are essentially the best available [43] with which to represent the real geometry of ether linked dimers.

This leaves the molar interaction parameters ε_{AA} and ε_{cc} which we have obtained by fitting the calculated nematic-isotropic transition temperatures to the experimental values for the three series of symmetric dimers (the BCBO*n* and *m*.O*n*O.*m* with $m=2$ and 6). The results of this fitting procedure are shown in figures 39, 40 and 41 for the BCBO*n*, 2.O*n*O.2 and 6.O*n*O.6 series, respectively. The overall agreement between theory and experiment is quite good especially in view of the approximations built into the Marcelja–Luckhurst theory. Thus, the initial strong alternation in T_{NI} with the spacer length followed by its attenuation is predicted by the theory. For the BCBO*n* series (see figure 39), the initial alternation is predicted to be slightly smaller than that observed, but then becomes slightly larger as the spacer length is increased. This slight disagreement may well result from the scaling of the strength parameters in equation (8) by the molar volume; use of an exponent different to -1 might well improve the agreement. This is certainly found when using Maier–Saupe theory to fit the temperature dependence of the orientational order parameter at constant pressure [44], although under certain circumstances this does contravene statistical mechanical consistency [45, 46]. The agreement for the 2.O*n*O.2 series (see figure 40) is as good as for the BCBO*n* series, with the marked exception of 2.O3O.2 where the observed T_{NI} is significantly lower than that predicted. We have no explanation for this failure. The theory seems to work best for the 6.O*n*O.6 series (see figure 41), although this may well be an artifact resulting from the flexibility of the terminal chain. This flexibility was

Downloaded At: 10:48 26 January 2011

excluded from our calculations because of the dramatic increase in the computational resources which its inclusion would demand. We should note that although some members of the 6.O*n*O.6 series exhibit S_A–I transitions, experience shows that the alternation in T_{S_AI} for later members of a series parallels that for T_{NI} observed for earlier members of the same series, as we had noted previously.

The optimum value of the molar parameters ε_{AA}, ε_{BB}, and ε_{cc} used to obtain the theoretical plots shown in figures 39–41 are given in table 10. The interaction parameter for the mesogenic group increases from cyanobiphenylyl to benzylidene-4′-ethylaniline to benzylidene-4′-*n*-hexylaniline. However, much of this increase can be associated with the increase in the molar volume of the mesogenic group which is also included in table 10. Thus the ratio ε_{AA}/V_m is essentially constant as might be expected for mesogenic groups with essentially the same anisotropies. The carbon–carbon interaction parameter ε_{cc} also changes from one series of symmetric dimers to the next. Such a variation is not expected and reveals an undesirable feature in the Marcelja–Luckhurst theory in that the interaction parameters are not strictly transferable. To overcome this difficulty when calculating the transitional properties of the non-symmetric dimers, we have averaged the values of ε_{cc} for the particular pairs; these averages are given in table 11. Since we wish to compare the transition temperatures for

Downloaded At: 10:48 26 January 2011

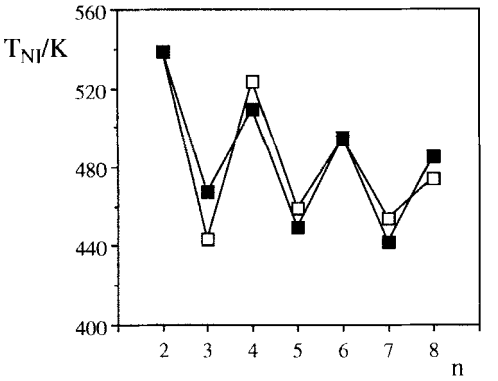

Figure 39. The dependence of the experimental (□) and calculated (■) nematic–isotropic transition temperatures on the number of methylene units in the flexible alkyl spacer for the BCBO*n* series.

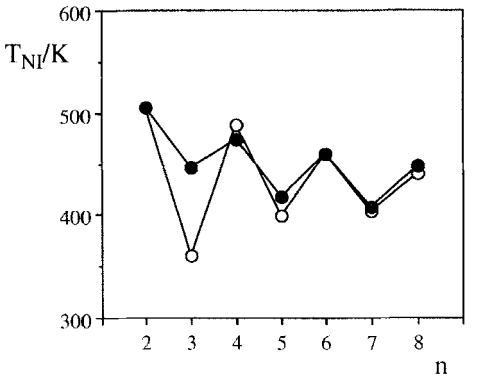

Figure 40. The dependence of the experimental (○) and calculated (●) nematic–isotropic transition temperatures on the number of methylene units in the flexible alkyl spacer for the 2.O*n*O.2 series.

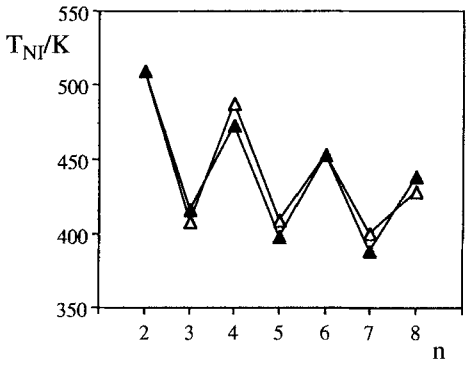

Figure 41. The dependence of the experimental (△) and calculated (▲) nematic–isotropic transition temperatures on the number of methylene units in the flexible alkyl spacer for the 6.O*n*O.6 series.

Table 10. The optimized values of the molar segmental interaction parameters and the molar volumes of the mesogenic groups.

	Series		
	BCBO*n*	2.O*n*O.2	6.O*n*O.6
ε_{AA}/kJ cm^3	1·61	1·83	2·48
ε_{cc}/kJ cm^3	0·076	0·058	0·038
V_A/cm^3 mol^{-1}	109·6	132·4	173·4

Table 11. The averaged carbon–carbon interaction parameters and the recalculated values of the mesogenic group parameters.

	System	
	BCBO*n*/2.O*n*O.2	BCBO*n*/6.O*n*O.6
ε_{AA}/kJ cm^3	1·65|1·77	1·71|2·36
ε_{cc}/kJ cm^3	0·067	0·057

the non-symmetric dimers with those for the symmetric dimers, we have recalculated these T_{NI} using the averaged values for ε_{cc} and adjusted the value for ε_{AA} to obtain the best agreement with experiment. Given the new constraint on ε_{cc}, agreement with experiment is not quite as good as that shown in figures 39–41 when ε_{cc} was allowed to vary.

With the parameters given in table 11 we can now calculate the transition temperatures for the non-symmetric dimers CB.O*n*O.2 and CB.O*n*O.6. The results of these calculations are shown in figures 42 and 43, together with the experimental clearing temperatures. The agreement between theory and experiment is really quite encouraging given that there were no adjustable parameters in the calculations. The agreement is slightly better for the CB.O*n*O.6 series than for the CB.O*n*O.2, in keeping with our observations for the symmetric dimers. From these results for the clearing

Downloaded At: 10:48 26 January 2011

temperatures of the non-symmetric dimers and those obtained for the symmetric dimers using the same interaction parameters, we can calculate the scaled shifted temperatures ΔT_{SC}. These are shown in figure 44 for the CB.O*n*O.2 and in figure 45 for the CB.O*n*O.6 series. We can see that for the short terminal chain, ΔT_{SC} is predicted to be small and negative; it also exhibits a modest alternation. This contrasts with the experimental results shown in figure 32 where ΔT_{SC} is found to be positive, except for CB.O8O.2 where ΔT_{SC} is negative. Theory on the other hand predicts ΔT_{SC} for this member of the series to be small but positive. The theoretical results for the CB.O*n*O.6 series in figure 45 show that ΔT_{SC} is larger, starting positive (for $n=2$) and then becoming increasingly negative as the spacer length increases. This predicted behaviour is exactly opposite to that shown in figure 32, where ΔT_{SC} is initially negative and then increases with the length of the spacer.

What significance should we attach to this qualitative disagreement between the observed values of ΔT_{SC} and those predicted by the Marcelja–Luckhurst theory? As we have seen the theory is able to predict the variation of the nematic–isotropic transition temperatures along a series of dimers in quite reasonable agreement with experiment; the qualitative features are certainly well reproduced. We might, therefore, have expected that the dependence of ΔT_{SC} on the length of the flexible spacer would also be

Downloaded At: 10:48 26 January 2011

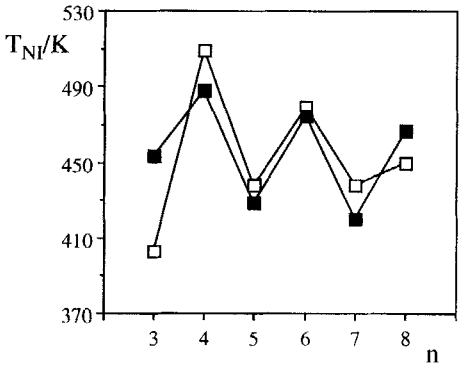

Figure 42. The dependence of the experimental (□) and calculated (■) nematic–isotropic transition temperatures on the number of methylene units in the flexible alkyl spacer for the CB.O*n*O.2 series.

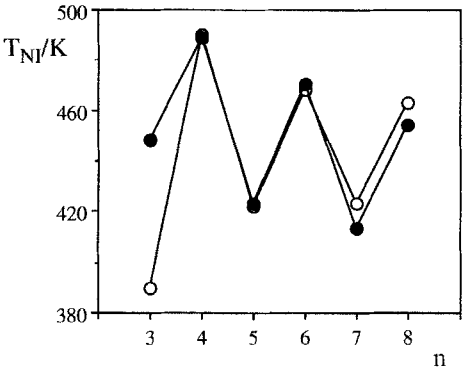

Figure 43. The dependence of the experimental (○) and calculated (●) nematic–isotropic transition temperatures on the number of methylene units in the flexible alkyl spacer for the CB.O*n*O.6 series.

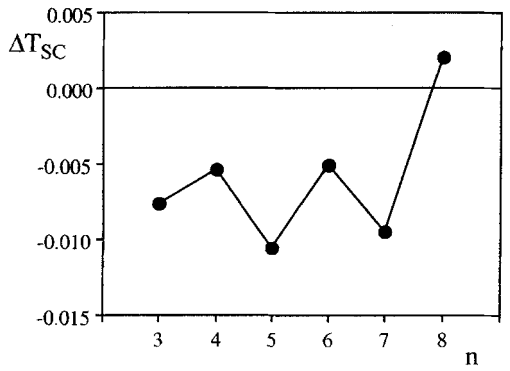

Figure 44. The dependence of the scaled shifted transition temperatures ΔT_{SC} on the number of methylene units in the flexible alkyl spacer for the CB.O*n*O.2 series.

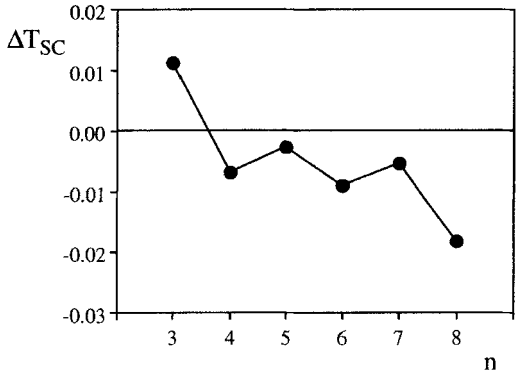

Figure 45. The dependence of the scaled shifted transition temperatures ΔT_{SC} on the number of methylene units in the flexible alkyl spacer for the CB.O*n*O.6 series.

Downloaded At: 10:48 26 January 2011

accounted for, at least qualitatively. This is especially the case because the approximations in the theory should influence the individual transition temperatures more or less equally and so result in a more accurate prediction of ΔT_{SC}, which depends essentially on a ratio of transition temperatures. The failure of the theory must, we believe, result from one of the fundamental approximations involving the non-symmetric dimers in a qualitatively different way to the symmetric dimers. The most obvious candidate is the geometric mean approximation for the mixed strength parameter ε_{AB} (see quation (9)). If charge-transfer interactions are important, as the results for the layer spacing suggest, then we should certainly expect ε_{AB} to differ from the geometric mean of ε_{AA} and ε_{BB}. Such deviations are certainly predicted to result in shifts in the transition temperatures for binary nematogenic mixtures [44]. It is to be anticipated that they should also cause similar deviations for the non-symmetric dimers. We have not been able to confirm this expectation because relaxing the geometric mean approximation results in a dramatic increase in the computational complexity of the calculations. Nonetheless, it would seem that the failure of the Marcelja–Luckhurst theory to account for the ΔT_{SC} provides further support for the importance of charge-transfer interactions in determining the behaviour of the non-symmetric dimers.

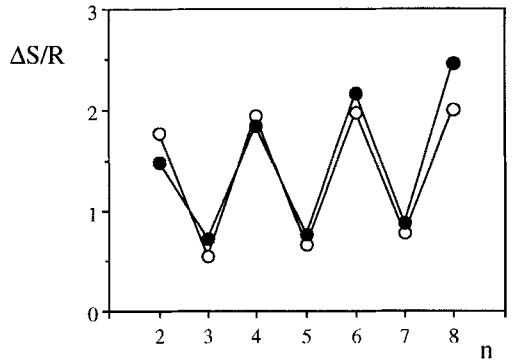

Figure 46. The dependence of the experimental (○) and calculated (●) nematic–isotropic transitional entropies on the number of methylene units in the flexible spacer for the BCBO*n* series.

Downloaded At: 10:48 26 January 2011

Another transitional property which is predicted by the theory is the entropy change at the nematic–isotropic transition. Such predictions are of particular interest here because, although all of the dimers, both symmetric and non-symmetric, exhibit the characteristic unattenuated alternation with the length of the flexible spacer, the particular values of $\Delta S/R$ vary with the nature of the mesogenic groups (see figures 18, 20 and 26). The predicted entropies of transition are shown for the BCBO*n* series in figure 46; these were calculated using the parameters in table 11. The alternation is clearly apparent and is in reasonable agreement with experiment; the theory also predicts the general increase in $\Delta S/R$ as the spacer length is increased and the absence of any marked attenuation. We have also calculated the transitional entropies for the two series of symmetric Schiff's base dimers. The results of these calculations are indistinguishable from those for the cyanobiphenylyl dimers and so they have not been plotted in figure 46. In contrast to the theory, the experimental $\Delta S/R$ exhibit a quite marked dependence on the nature of the mesogenic group. Given the symmetric nature of the dimers we cannot attribute this failure of the Marcelja–Luckhurst theory to charge-transfer interactions. Instead, we believe that it results from deviations of the interaction tensors for the mesogenic groups from the cylindrical symmetry assumed for them. Indeed the biaxiality of rigid molecules is known to lower the nematic–isotropic transitional entropy from the limiting value found for cylindrically symmetric molecules. The estimation of the biaxiality in the interaction strength tensor for the mesogenic group from its geometry is a challenging task. It seems likely that the recently introduced surface tensor parametrization of the potential of mean torque [47] (see equation (2)) could be used to perform this task and we are now exploring this possibility. Our preliminary calculations have shown that the entropy change at the nematic–isotropic transition is indeed sensitive to the geometry of the biphenyl group, as reflected by the torsional angle between the two rings; as the angle increases from 45° to 90°, so the transitional entropy also increases by $\Delta S/R$ of about 0·5, at least for even members of the series. Further speculation, however, must await the completion of these calculations.

3.4. *Binary mixtures of 2.OnO.2 with BCBO*n

We have now seen that the thermal properties of the non-symmetric dimers in many instances approach the arithmetic mean of those of the parent symmetric dimers, but the structure of the intercalated smectic A phase apparently arises from the interaction

between the unlike mesogenic species. This prompts the question as to how important is it for the differing mesogenic groups to be chemically linked by a spacer, or can the same smectic structures be observed for binary mixtures of symmetric dimers. In these studies we have investigated mixtures of the 2.O*n*O.2 and BCBO*n* series; this choice was made as the mixed mesogenic group interaction appears to be most important in determining the properties of materials having short terminal chains. The phase diagrams were constructed by determining the transitional properties of mixtures and not by the contact method. Thorough mixing of the two components is crucial for such studies and was achieved by blending in the molten state. The transition temperatures of the mixtures were recorded using a polarizing microscope equipped with a hot-stage at a heating rate of $1°C\,min^{-1}$.

The phase diagram for binary mixtures of 2.O5O.2 and BCBO5 is shown as figure 47. A eutectic mixture is formed at 0·45 mol fraction of 2.O5O.2 and 92°C and compares well with the predicted values using the Schröder–van Laar equation of 0·50 and 108°C, respectively. A small biphasic region is present at the nematic–isotropic transition in all the phase diagrams we have studied, as expected for first order phase transitions. It is interesting to note that no smectic behaviour is observed in these mixtures, although the non-symmetric dimer CB.O5O.2 exhibits a monotropic smectic A phase. However, T_{SAN} for CB.O5O.2 is 83°C, which lies below the eutectic point for the binary mixture. It should be noted that the nematic–isotropic phase boundary in figure 47, as well as in figures 48 and 49, exhibits an upward curvature suggesting a positive deviation in ε_{AB} away from the geometric mean approximation as expected, and observed for other mixtures. Smectic behaviour is observed in mixtures of 2.O6O.2 and BCBO6 as shown in figure 48. The smectic A–nematic transition temperatures for the mixtures are only slightly greater than for the analogous non-symmetric dimer CB.O6O.2 for which T_{SAN}

Downloaded At: 10:48 26 January 2011

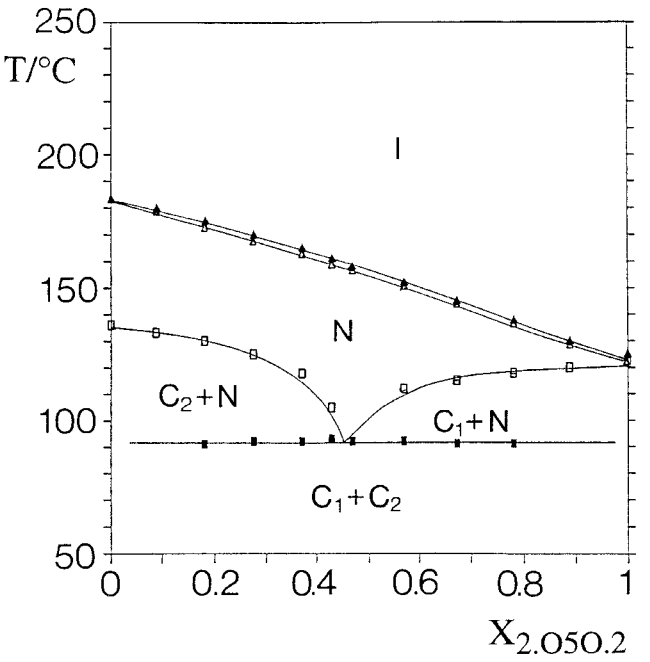

Figure 47. The phase diagram for binary mixtures of 2.O5O.2 and BCBO5.

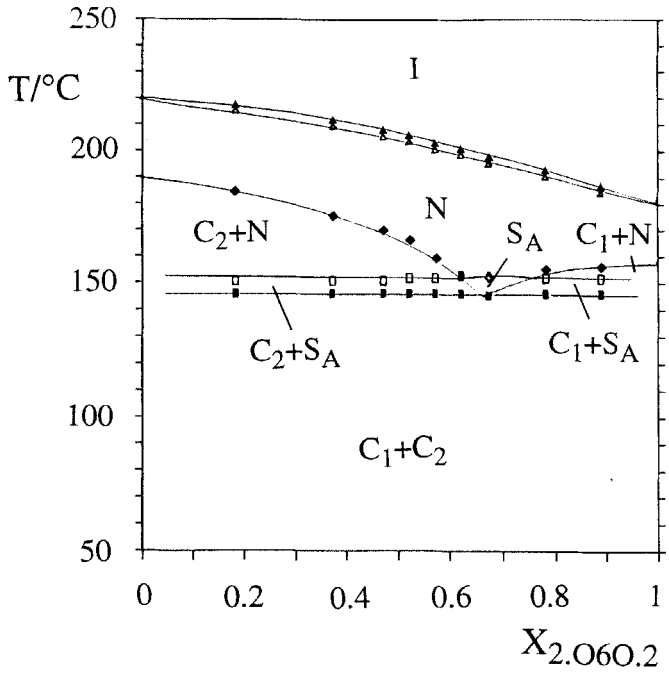

Figure 48. The phase diagram for binary mixtures of 2.O6O.2 and BCBO6.

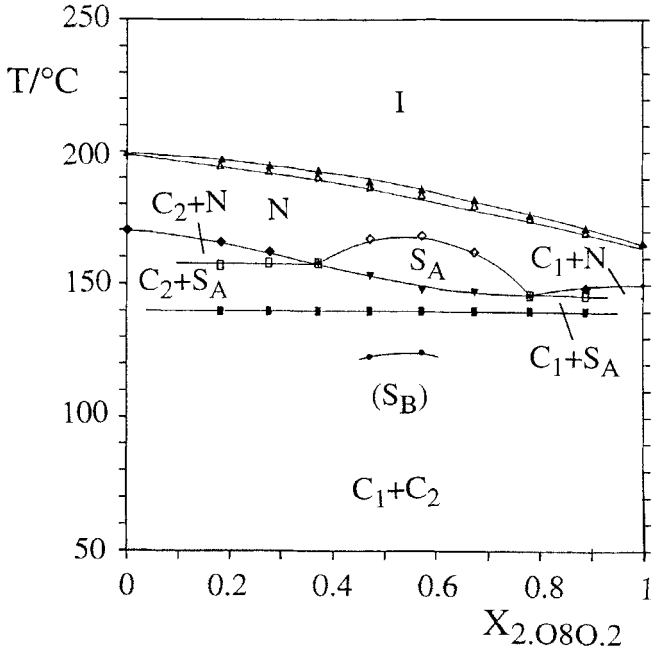

Figure 49. The phase diagram for binary mixtures of 2.O8O.2 and BCBO8.

Downloaded At: 10:48 26 January 2011

Table 12. The smectic A periodicity, d, and the estimated all-*trans* molecular lengths, l_A for the 2.O*n*O.2 series, l_B for BCBO10 and l, the arithmetic mean of l_A and l_B for equimolar binary mixtures of members of the 2.O*n*O.2 series and BCBO10.

n	T/°C	d/Å	l_A/Å	l_B/Å	l/Å	d/l
2	140	19·4	42·0	36·4	39·2	0·49
3	145	20·0	44·0	36·4	40·2	0·50
4	142	20·7	46·8	36·4	41·6	0·50
5	146	21·4	48·8	36·4	42·6	0·50
6	144	22·0	51·4	36·4	43·9	0·50

is 149°C. The phase diagram for 2.O8O.2 and BCBO8, shown as figure 49, depicts smectic behaviour over wider concentration and temperature ranges, although does not indicate a eutectic mixture. A monotropic hexatic B, as well as smectic A phases are observed. These smectic phases were investigated using X-ray diffraction and for a mixture containing 0·6 mol fraction of 2.O8O.2 the layer spacing in the smectic A phase was 18·5 Å at 160°C and in the hexatic B phase 18·7 Å at 120°C. These values compare to the mean of the estimated all-*trans* molecular lengths of the two components of 37 Å which clearly indicates an intercalated structure. The maximum thermal stability of the smectic A phase is located around the equimolar mixture and this supports the view that the driving force for phase formation is the mixed mesogenic unit interaction. It is interesting to note that the maximum thermal stability is greater than that of the analogous non-symmetric dimer CB.O8O.2. This suggests that the mixed interaction is more effective in the mixture and that the spacer has less influence on the phase structure. Table 12 lists the layer spacings for the smectic A phases, as well as the molecular lengths for several equimolar mixtures of members of the 2.O*n*O.2 series and BCBO10, and it is clear that the layer spacing in each case is approximately half the average molecular length of the components. This suggests that these also form intercalated phases, although it is difficult to visualize the molecular arrangement in the smectic A phase for the 2.O2O.2 and BCBO10 mixture in which the molecular lengths of the components are significantly different, unless we allow for a relatively low degree of translational order.

Downloaded At: 10:48 26 January 2011

Summary

Six new series of the CB.O*n*O.*m* family of compounds have been prepared and exhibit smectic behaviour unique to this general class of materials, namely non-symmetric dimeric liquid crystals. This investigation includes the identification of several new smectic modifications, namely, the intercalated smectic C and I phases, and the intercalated crystal B and J phases. In consequence, we believe that these materials will be valuable in structural studies of smectic phases as well as in investigations of novel phase transitions. We propose that the current smectic nomenclature be extended to include these new structural variants and denote the intercalated packing arrangement by a subscript c. The intercalated smectic phases are thought to arise from a specific interaction between the unlike mesogenic groups. Such structures are prevented from forming, however, if the terminal chain cannot be accommodated into the intercalated structure and this accounts for the unusual dependence of the smectic thermal stability on the length of the terminal chain. The tilt direction in the intercalated smectic C phase alternates between adjacent layers. It is analogous in this respect to the S_{C_2} phase exhibited by certain semi-flexible main-chain liquid crystal

polymers and also the antiferroelectric smectic C phases. This important similarity should be denoted using an appropriate label and we suggest a superscript † for this purpose. The existence of a specific interaction between the mesogenic groups is suggested also by calculations of the transition temperatures using the Marcelja–Luckhurst theory. The behaviour of binary mixtures of the symmetric dimers appears, in part, to be governed by the mixed mesogenic group interaction, suggesting that the chemical linking of the two groups is not an important factor in determining phase behaviour or phase structure as intercalated structures are exhibited also by the mixtures. The molecular packing within a layer in order to maximize this mixed interaction is difficult to visualize and speculation must await the results of further experiments.

We wish to thank the Royal Commission for the Exhibition of 1851 for the award of a fellowship to Dr C. T. Imrie and the Science and Engineering Research Council for research studentships to Dr R. W. Date, Dr L. Taylor and Mr S. J. Roskilly as well as for a grant, GR/C/95428, towards the cost of the equipment used in this investigation.

Downloaded At: 10:48 26 January 2011

References

[1] DEMUS, D., 1990, *Liq. Crystals*, **5**, 75.
[2] EMSLEY, J. W., LUCKHURST, G, R., SHILSTONE, G. N., and SAGE, I., 1984, *Molec. Crystals liq. Crystals Lett.*, **102**, 223.
[3] HOGAN, J. L., IMRIE, C. T., and LUCKHURST, G. R., 1988, *Liq. Crystals*, **3**, 645.
[4] ATTARD, G. S., GARNETT, S., HICKMAN, C. G., IMRIE, C. T., and TAYLOR, L., 1990, *Liq. Crystals*, **7**, 495.
[5] IMRIE, C. T., 1989, *Liq. Crystals*, **6**, 391.
[6] GRIFFIN, A. C., and VAIDYA, S. R., 1988, *Liq. Crystals*, **3** 1275.
[7] IKEDA, T., MIYAMOTO, T., KURIHARA, S., TSUKADA, M., and TAZUKE, S., 1990, *Molec. Crystals liq. Crystals* B, **182**, 357.
[8] ATTARD, G. S., IMRIE, C. T., and KARASZ, F. E., 1992, *Chem. Mater.*, **4**, 1246.
[9] DATE, R. W., IMRIE, C. T., LUCKHURST, G. R., and SEDDON, J. M., 1992, *Liq. Crystals*, **12**, 203.
[10] CRIVELLO, J. V., DEPTOLLA, M., and RINGSDORF, H., 1988, *Liq. Crystals*, **3**, 235.
[11] KELLER, P., and LIEBERT, L., 1978, *Solid. St. Phys.*, Suppl. **14**, 19.
[12] GRAY, G. W., and GOODBY, J. W., 1984, *Smectic Liquid Crystals—Textures and Structures* (Leonard-Hill).
[13] DEMUS, D., and RICHTER, L., 1978, *Textures of Liquid Crystals* (Verlag Chemie).
[14] WATANABE, J., KOMURA, H., and NIIORI, T., 1993, *Liq. Crystals*, **13**, 455.
[15] GOODBY, J. W., NISHIYAMA, I., SLANEY, A. J., BOOTH, C. J., and TOYNE, K. J., 1993, *Liq. Crystals*, **14**, 37.
[16] TOURNILHAC, F. G., BOSIO, L., SIMON, J., BLINOV, L. M., and YABLONSKY, S. V., 1993, *Liq. Crystals*, **14**, 405.
[17] TOURNILHAC, F., BOSIO, L., NICOUD, J. F., and SIMON, J., 1988, *Chem. Phys. Lett.*, **145**, 452.
[18] TOURNILHAC, F., BLINOV, L. M., SIMON, J., and YABLONSKY, S. V., 1992, *Nature, Lond.*, **359**, 621.
[19] LEADBETTER, A. J., FROST, J. C., and MAZID, M. A., 1979, *J. Phys. Lett., Paris*, **40**, L-325.
[20] COLLETT, J., SORENSEN, L. B., PERSHAN, P. S., LITSTER, J. D., BIRGENEAU, R. J., and ALS-NIELSEN, J., 1982, *Phys. Rev. Lett.*, **49**, 302.
[21] ABE, A., 1992 (private communication).
[22] EMSLEY, J. W., LUCKHURST, G. R., and SHILSTONE, G. N., 1984, *Molec. Phys.*, **53**, 1023.
[23] GANE, P. A. C., LEADBETTER, A. J., and WRIGHTON, P. G., 1981, *Molec. Crystals liq. Crystals*, **66**, 247.
[24] WATANABE, J., and HAYASHI, M., 1989, *Macromolecules*, **22**, 4083.
[25] TAKANISHI, Y., TAKEZOE, H., FUKUDA, A., KOMURA, H., and WATANABE, J., 1992, *J. mater. Chem.*, **2**, 71.
[26] WULF, A., 1978, *Molec. Crystals liq. Crystals*, **47**, 225.
[27] HUMPHRIES, R. L., JAMES, P. G., and LUCKHURST, G. R., 1971, *Symp. Faraday. Soc.*, **5**, 107.

[28] HUMPHRIES, R. L., and LUCKHURST, G. R., 1973, *Chem. Phys. Lett.*, **23,** 567.
[29] ATTARD, G. S., and IMRIE, C. T., 1992, *Liq. Crystals*, **11,** 785.
[30] FRENKEL, D., and MULDER, B. M., 1985, *Molec. Phys.*, **55,** 1171.
[31] ZARRAGOICOECHEA, E. J., LEVESQUE, D., and WEISS, J. J., 1992, *Molec. Phys.*, **75,** 989.
[32] FRENKEL, D., 1987, *J. phys. Chem.*, **91,** 4912.
[33] FRENKEL, D., 1988, *J. phys. Chem.*, **92,** 3280.
[34] GRAY, G. W., 1979, *The Molecular Physics of Liquid Crystals*, edited by G. R. Luckhurst and G. W. Gray (Academic Press), Chap. 1.
[35] IMRIE, C. T., and TAYLOR, L., 1989, *Liq. Crystals*, **6,** 1.
[36] GRAY, G. W., 1979, *The Molecular Physics of Liquid Crystals*, edited by G. R. Luckhurst and G. W. Gray (Academic Press), Chap. 12.
[37] BROWNSEY, G. J., and LEADBETTER, A. J., 1981, *J. Phys. Lett., Paris*, **42,** 135.
[38] MARCELJA, S., 1974, *J. chem. Phys.*, **60,** 3599.
[39] LUCKHURST, G. R., 1985, *Recent Advances in Liquid Crystalline Polymers*, edited by L. L. Chapoy (Elsevier), chap. 7.
[40] FLORY, P. J., 1969, *Statistical Mechanics of Chain Molecules* (Wiley Interscience).
[41] LUCKHURST, G. R., ZANNONI, C., NORDIO, P. L., and SEGRE, U., 1975, *Molec. Phys.*, **30,** 1345.
[42] BONDI, A., 1964, *J. phys. Chem.*, **68,** 441.
[43] COUNSELL, C. R. J., EMSLEY, J. W., LUCKHURST, G. R., and SACHDEV, H. S., 1988, *Molec. Phys.*, **63,** 33.
[44] HUMPHRIES, R. L., JAMES, P. G., and LUCKHURST, G. R., 1972, *J. chem. Soc. Faraday Trans, II*, **68,** 1031.
[45] COTTER, M. A., 1977, *Molec. Crystals liq. Crystals*, **39,** 173.
[46] EMSLEY, J. W., LUCKHURST, G. R., and SMITH, S. W., 1990, *Molec. Phys.*, **70,** 967.
[47] FERRARINI, A., MORO, G. J., NORDIO, P. L., and LUCKHURST, G. R., 1992, *Molec. Phys.*, **77,** 1. FERRARINI, A., LUCKHURST, G. R., NORDIO, P. L., and ROSKILLY, S. I., 1994, *J. chem. Phys.* (in the press).

Downloaded At: 10:48 26 January 2011